ELSEVIER

Precambrian Research 120 (2003) 279–325

Precambrian Research

www.elsevier.com/locate/precamres

Chemostratigraphy of Paleoproterozoic carbonate successions of the Wyoming Craton: tectonic forcing of biogeochemical change?

A. Bekker [a,*], J.A. Karhu [b], K.A. Eriksson [a], A.J. Kaufman [c]

[a] *Department of Geological Sciences, Virginia Polytechnic Institute and State University, Blacksburg, VA 24061, USA*
[b] *Department of Geology, University of Helsinki, P.O. Box 64, FIN-00014 Helsinki, Finland*
[c] *Department of Geology, University of Maryland at College Park, College Park, MD 20742, USA*

Accepted 11 October 2002

Abstract

The Archean Wyoming Craton is flanked on the south and east by belts of Paleoproterozoic supracrustal successions whose correlation is complicated by lack of geochronologic constraints and continuous outcrop. However, carbonate units in these successions may be correlated by integrating carbon isotope stratigraphy with lithostratigraphy. The ~10 km thick Paleoproterozoic Snowy Pass Supergroup in the Medicine Bow Mountains was deposited on the present-day southern flank of the Wyoming Craton; it contains three discrete levels of glacial diamictite correlative with those in the Huronian Supergroup, on the southern margin of the Superior Craton. The Nash Fork Formation of the upper Snowy Pass Supergroup is significantly younger than the uppermost diamictite and was deposited after the end of the Paleoproterozoic glacial epoch. Carbonates at the base of the Nash Fork Formation record remarkable ^{13}C-enrichment, up to +28‰ (V-PDB), whereas those from overlying members of the lower Nash Fork Formation have δ^{13}C values between +6 and +8‰. Carbonates from the upper Nash Fork Formation above the carbonaceous shale have carbon isotope values ranging between 0 and +2.5‰. The transition from high carbon isotope values to those near 0‰ in the Nash Fork Formation is similar to that at the end of the ca. 2.2–2.1 Ga carbon isotope excursion in Fennoscandia. This chemostratigraphic trend and deposition of BIFs, Mn-rich lithologies, carbonaceous shales and phosphorites at the end of the global ca. 2.2–2.1 Ga carbon isotope excursion are likely related to ocean overturn associated with the final breakup of the Kenorland supercontinent. Correlative carbonates from the Slaughterhouse Formation in the Sierra Madre, WY, and from the Whalen Group in the Rawhide Creek area in the Hartville Uplift, WY, have highly positive carbon isotope values. In contrast, carbonates from other exposures of the Whalen Group in the Hartville Uplift and all carbonate units in the Black Hills, SD, have carbon isotope values close to 0‰. Combined with existing geochronologic and stratigraphic constraints, these data suggest that the Slaughterhouse Formation and the succession exposed in the Rawhide Creek area of the Hartville Uplift are correlative with the lower and middle Nash Fork Formation and were deposited during the ca. 2.2–2.1 Ga carbon isotope excursion. The Estes and Roberts Draw formations in the Black Hills and carbonates from other exposures in the Hartville Uplift postdate the ca. 2.2–2.1 Ga

* Corresponding author. Present address: Department of Earth and Planetary Sciences, Harvard University, 20 Oxford Street, Cambridge, MA 02138, USA. Fax: +1-617-495-8839

E-mail address: abekker@fas.harvard.edu (A. Bekker).

0301-9268/02/$ - see front matter © 2002 Elsevier Science B.V. All rights reserved.
PII: S0301-9268(02)00164-X

positive carbon isotope excursion and are most likely correlative with the upper Nash Fork Formation. The passive margin, on which the carbonates with highly positive carbon isotope values were deposited, extended around the southern flank of the Wyoming Craton through the Sierra Madre, Medicine Bow Mountains and Hartville Uplift. The presence of carbonates with carbon isotope values close to 0‰ in the upper Nash Fork Formation and the Whalen Group indicates that the passive margin persisted on the southern flank of the Wyoming Craton after the carbon isotope excursion. Rifting in the Black Hills, likely related to the final breakup of the Kenorland, succeeded the carbon isotope excursion, since the Estes and Roberts Draw formations, deposited during rifting and ocean opening on the eastern flank of the Wyoming Craton, postdate the carbon isotope excursion.
© 2002 Elsevier Science B.V. All rights reserved.

Keywords: Chemostratigraphy; Paleoproterozoic; Biogeochemistry; Kenorland; Wyoming

1. Introduction

Correlation of Precambrian sedimentary successions lacking biostratigraphic control is greatly hindered by the general absence of radiometric age constraints, as well as metamorphic and diagenetic overprinting. It may be possible to overcome these limitations by a focus on event stratigraphy, based on the study of well-preserved marker beds that represent stratigraphic expressions of global events. This approach may be particularly useful for Paleoproterozoic sedimentary successions insofar as the 2.5–2.0 Ga exosphere was affected by a number of distinct tectonic, climatic, and biogeochemical perturbations. These events include:

1) A 2.48–2.45 Ga superplume event expressed in the rock record by large igneous provinces with mafic volcanic and plutonic rocks, initiation of rifting, and worldwide deposition of banded iron formations (Amelin et al., 1995; Heaman, 1997; Barley et al., 1997; Kump et al., 2000);
2) An extended glacial epoch (ca. 2.45–2.3 Ga; Young, 1991) accompanied by carbon isotope excursions (Bekker et al., 1999, 2001a);
3) A period of enhanced weathering after the end of the Paleoproterozoic glacial epoch (Young, 1973; Marmo, 1992);
4) A second superplume event around 2.25 Ga that formed extensive plateau basalts and dikes, and led to the second stage of rifting and the breakup along some rift systems (Cadman et al., 1993; Lanyon et al., 1993; Cornell et al., 1996; Buchan et al., 1998; Davis, 1997; Martin et al., 1998);
5) A major carbon isotope excursion between ca. 2.2–2.1 Ga not associated with a known glaciation (Karhu and Holland, 1996);
6) A great oxidation event (Karhu and Holland, 1996), and
7) Final breakup of the Kenorland supercontinent at 2.1–2.0 Ga (Aspler and Chiarenzelli, 1998).

Sedimentary rift successions associated with the initial breakup of the Kenorland supercontinent contain detrital uraninite and pyrite (Kirkham and Roscoe, 1993). Atmospheric pO_2 may have changed episodically during the glacial epoch in response to fluctuations in the exogenic carbon cycle (Bekker et al., 2001a). Worldwide, the end of the Paleoproterozoic glacial epoch was followed by deposition of mature, Al-rich quartzites suggesting a climate change to greenhouse conditions favoring chemical weathering (Young, 1973; Karlstrom et al., 1983; Marmo, 1992; Schreiber and Eriksson, 1992; Gutzmer and Beukes, 1996; Ojakangas, 1997). The ca. 2.2–2.1 Ga carbon isotope excursion (Karhu and Holland, 1996) also succeeded the glacial epoch but the temporal and stratigraphic relationship between the beginning of the carbon isotope excursion and deposition of mature quartzites is poorly constrained. The carbon isotope excursion is thought to have lasted more than 100 million years and was likely accompanied by an increase in atmospheric oxygen (Karhu and Holland, 1996). Carbonate successions deposited during this interval contain pseudomorphs of anhydrite and gypsum (Akhmedov, 1990; Bekker, 1998; El Tabakh et al., 1999; Bekker and Eriksson, in press) suggesting warm

and arid climates. The end of the carbon isotope excursion on the Fennoscandian Shield (between 2062±2 and 2113±4 Ma) was accompanied by voluminous mafic volcanism, which has been related to supercontinent breakup (Karhu, 1993). Deposition of BIFs, phosphorites, Mn-rich sediments, and organic-rich shales with high organic carbon contents (and $\delta^{13}C$ as low as −40 to −45‰) coincides with the end of the carbon isotope excursion on the Fennoscandian Shield (Karhu, 1993; Melezhik et al., 1999b). Melezhik et al. (1997a) also noticed a temporal relationship between the end of biogeochemical event and the decline in stromatolite abundance and diversity on the Fennoscandian Shield. The Fennoscandian chemostratigraphic record for the end of the carbon isotope excursion, however, lacks high resolution due to discontinuous outcrops and a prominent unconformity (Melezhik et al., 1999b). Thus a detailed record from a different, but broadly coeval basin, of carbon isotope variations and accompanying lithological and geochemical changes at the end of the biogeochemical anomaly would help to constrain whether these events were local or global, and further understand their causes.

This paper presents new chemostratigraphic data for the Nash Fork Formation of the Snowy Pass Supergroup, WY, which was deposited after the end of the Paleoproterozoic glacial epoch, and broadly equivalent Paleoproterozoic supracrustal successions of the Sierra Madre and Hartville Uplift, WY, and Black Hills, SD (Fig. 1). The paper has four objectives: (1) to provide a high-resolution record of temporal $\delta^{13}C$ and lithological changes at the end of the ca. 2.2–2.1 Ga carbon isotope excursion; (2) to test earlier proposed lithostratigraphic correlations and to constrain the age of the studied units based on chemostratigraphic data; (3) to incorporate these new age constraints and correlations into our understanding of the tectonic history of the Wyoming Craton; and (4) to compile evidence that secular carbon isotope changes at the end of the ca. 2.2–2.1 Ga carbon isotope excursion were accompanied by a number of perturbations in ocean composition, and that these are, most likely, related to global tectonics.

2. Regional geology and stratigraphy

The Wyoming Craton is a triangular block of Archean crust surrounded by isolated Paleoproterozoic mobile belts. Paleoproterozoic sedimentary and subordinate volcanic rocks are well exposed on the southeastern margin of the Wyoming Craton in the Sierra Madre and Medicine Bow Mountains, WY, as well as in the Black Hills, SD (Fig. 1). These rocks were deformed during the 1.78–1.74 Ga Medicine Bow Orogeny when the southern passive margin of the Wyoming Craton collided along the Cheyenne Belt Suture with island arcs approaching from the south (Karlstrom and Houston, 1984; Chamberlain, 1998; Dahl and Frei, 1998). The Cheyenne Belt is well exposed in the Sierra Madre and Medicine Bow Mountains and is traceable to the east through the Laramie Mountains and Richeau Hills; further to the east it disappears under Phanerozoic cover where it can only be inferred from geophysical data (Sims, 1995). The projection of the Cheyenne Belt and, therefore, the Proterozoic passive margin passes south of the Hartville Uplift (Fig. 1). The eastern margin of the Wyoming Craton is bounded by the Black Hills collisional orogen (Redden et al., 1990; Sims, 1995; Dahl and Frei, 1998).

Volcano-sedimentary rocks in the Medicine Bow Mountains are grouped into the Snowy Pass Supergroup that unconformably overlies or is in fault contact with the Late Archean basement. The Snowy Pass Supergroup in the Medicine Bow Mountains is the thickest and the most extensive Paleoproterozoic succession of the Wyoming Craton (Fig. 1). Deposition of the supergroup on the southern flank of the Wyoming Craton followed the initial rifting of the Kenorland supercontinent at ca. 2.45 Ga. The supergroup contains a basal siliciclastic rift succession with detrital uraninite and pyrite deposited in a fluvial setting, followed by three stratigraphically discrete diamictite horizons and passive margin sediments (Fig. 2; Houston et al., 1992). A transition from rift to open marine conditions occurred at the level of the Vagner Formation before the end of the glacial epoch (Karlstrom et al., 1983). The youngest glacial horizon is overlain by thick, mature, Al-rich and hematite-bearing quartzites (Medicine

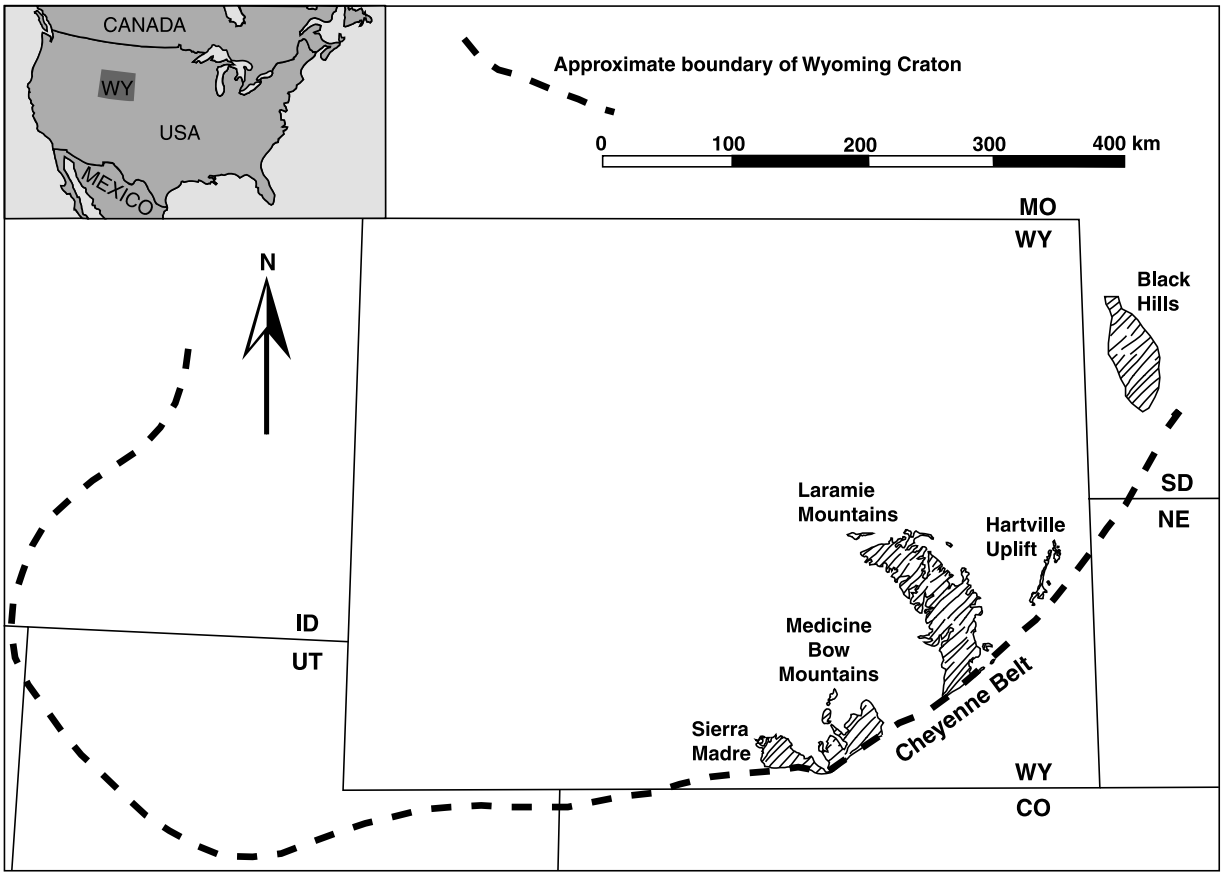

Fig. 1. Location of Paleoproterozoic sedimentary successions on the southeastern margin of the Wyoming Craton.

Peak Quartzite). The upper Libby Creek Group includes a thick carbonate succession (Nash Fork Formation), subaqueous mafic volcanic unit (Towner Greenstone) and, at the top, metapelites of the French Slate.

The Snowy Pass Supergroup forms broad open folds; the degree of metamorphism is greenschist facies, biotite grade (Houston et al., 1981). The age of the succession is constrained by U–Pb ages of detrital zircons from the base of the succession (Magnolia Formation) in the Sierra Madre Range and the age of the arc-continent collision in the Cheyenne Belt to between 2451 ± 9 Ma and 1.78–1.74 Ga (Karlstrom and Houston, 1984; Premo and Van Schmus, 1989; Chamberlain, 1998). The supergroup is subdivided by structural contacts (rotated thrust faults) into the Deep Lake Group and the lower and upper Libby Creek Group (Houston et al., 1992; see Fig. 2). Based on the presence of glaciogenic sediments in both the Deep Lake Group and the lower Libby Creek Group, Houston et al. (1992) assumed that only a small portion of the succession and a minor amount of time is missing along the Reservoir Lake fault; however, the Lewis Lake fault that separates the lower and upper Libby Creek Group might represent a major hiatus (Fig. 2).

The Deep Lake Group and the lower Libby Creek Group record rift and passive margin settings, whereas the upper Libby Creek Group reflects either a transition from a passive margin to a foredeep (Karlstrom et al., 1983), or a reactiva-

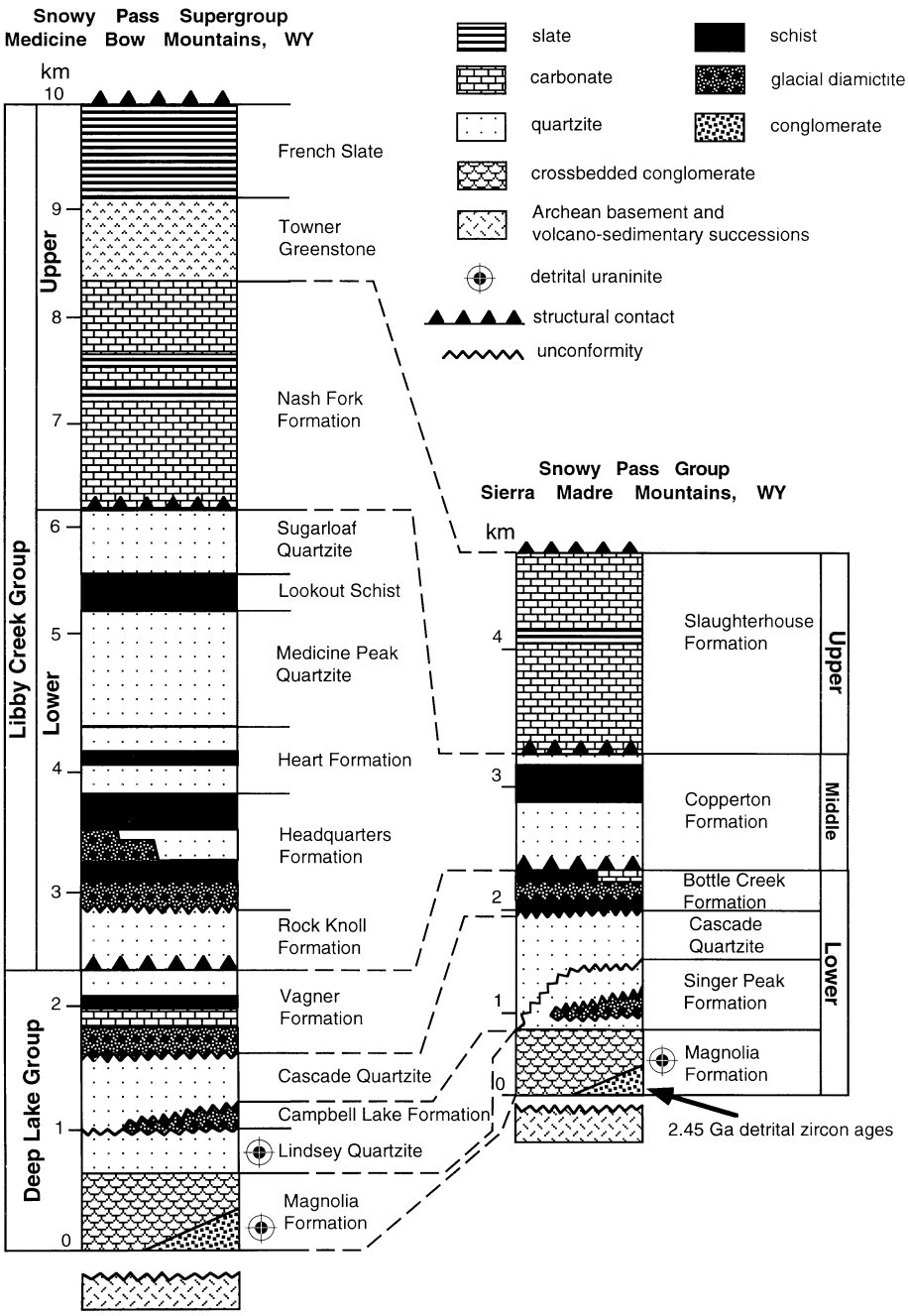

Fig. 2. Idealized stratigraphic column showing correlation between the Snowy Pass Supergroup, Medicine Bow Mountains, WY, and the Snowy Pass Group, Sierra Madre (after Houston et al., 1992). Detrital zircon age is after Premo and Van Schmus (1989).

tion of the mature passive margin (Bekker and Eriksson, in press). Mafic sills and dikes that range in composition from tholeiitic to calc-alkaline intrude the whole succession. Tholeiitic gabbros that intrude pre-folded Deep Lake Group and are likely related to rifting (Karlstrom et al., 1981)

were dated in the Sierra Madre and Laramie Mountains at 2.09–2.01 Ga (U–Pb zircon and baddeleyite; Premo and Van Schmus, 1989; Snyder et al., 1995; Cox et al., 2000). Evolution in dike and sill composition to calc-alkaline magmatism was related to a progressive change in the tectonic environment from rift to passive margin and to foredeep (Karlstrom et al., 1983). Pegmatitic metagabbro intruding the Cascade Quartzite of the Snowy Pass Group in the Sierra Madre was dated at 2092±9 Ma (U–Pb zircon; Premo and Van Schmus, 1989). The latter provides a minimum age for the Deep Lake Group in the Medicine Bow Mountains.

Correlation with other poorly exposed Paleoproterozoic supracrustal successions preserved along the flanks of the Wyoming Craton is tenuous, with the exception of the Snowy Pass Group in the Sierra Madre (Houston et al., 1992). The Paleoproterozoic succession in the Sierra Madre (Fig. 1) is strongly deformed and dismembered by a late cataclastic event (Houston, 1993) but, based primarily on lithostratigraphic similarities, it is considered to be correlative with the Snowy Pass Supergroup in the Medicine Bow Mountains (Houston et al., 1992; Fig. 2). Correlative horizons in these successions include a lower siliciclastic rift sequence with basal conglomerates containing detrital uraninite and pyrite, glacial diamictites, Al-rich mature quartzites, and thick carbonate units. The ca. 2.45 Ga age for the initiation of the Paleoproterozoic deposition on the southern flank of the Wyoming Craton is inferred from: (1) the minimum age of detrital zircon grains in the Magnolia Formation of the Sierra Madre (2451±9 Ma; Premo and Van Schmus, 1989); (2) the correlation with the Huronian Supergroup (Houston et al., 1992) for which the rifting age is well established at ca. 2.45 Ga (Krogh et al., 1984, 1996; Smith and Heaman, 1999), and (3) the age of the Baggot Rocks Granite in the Medicine Bow Mountains (2429±4 Ma; Premo and Van Schmus, 1989), which includes mafic dikes of the same age. Houston et al. (1992) proposed that carbonate rocks and carbonaceous phyllites of the Slaughterhouse Formation in the Sierra Madre are deep-water time-equivalents of the Nash Fork Formation in the Snowy Pass Supergroup (Fig. 2).

Paleoproterozoic rocks exposed in the Black Hills, South Dakota (Fig. 1) were deposited on the eastern flank of the Wyoming Craton and contain two rift successions overlain by passive-margin, back-arc, and foredeep deposits (Redden et al., 1990; Sims, 1995; note that Redden, pers. comm., 2002, interprets the Paleoproterozoic succession in the Black Hills as an intracratonic basin fill). Paleoproterozoic glaciogenic diamictites are lacking in the Black Hills possibly due to non-deposition or removal along the unconformity separating the two rift successions. Both rift successions are younger than the Archean Little Elk Granite that has a U–Pb zircon age of 2559±3 Ma (McCombs et al., 2001; Redden et al., 1990). The older rift succession was intruded by the Blue Draw Metagabbro (2170±120 Ma U–Pb zircon; Redden et al., 1990) and was then folded as well as eroded prior to deposition of the younger rift succession. The younger rift contains an older sequence dated at 1974.4±8 Ma (Ellison Formation; Redden et al., 1990), which is separated by an unconformity/disconformity from the younger sequence dated at 1884±29 Ma (Montana Mine Formation; Redden et al., 1990). The only carbonates older than the younger sequence are present within the siliciclastic deposits in the Nemo area in the northeastern part of the Black Hills (Fig. 3). Zircon overgrowths in Archean rocks have a highly discordant upper intercept Pb–Pb age of 2025±50 Ma likely related to thermal flux during the later rifting event (McCombs et al., 2001).

A volcano-sedimentary supracrustal succession named the Whalen Group outcrops in the Hartville Uplift (Fig. 1). The Whalen Group includes a thick carbonate succession and Lake Superior-type BIFs. The age of the Whalen Group is uncertain. Sims (1995) suggested a Paleoproterozoic age for the Whalen Group based on rarity of Archean platformal carbonates and Lake Superior-type BIFs on the Northern Hemisphere continents. Hofmann and Snyder (1985) described four types of stromatolites from the Whalen Group, two of which (*Hadrophycus* and *Gruneria*) are only known from Paleoproterozoic successions. Notably, the genus *Hadrophycus* was ori-

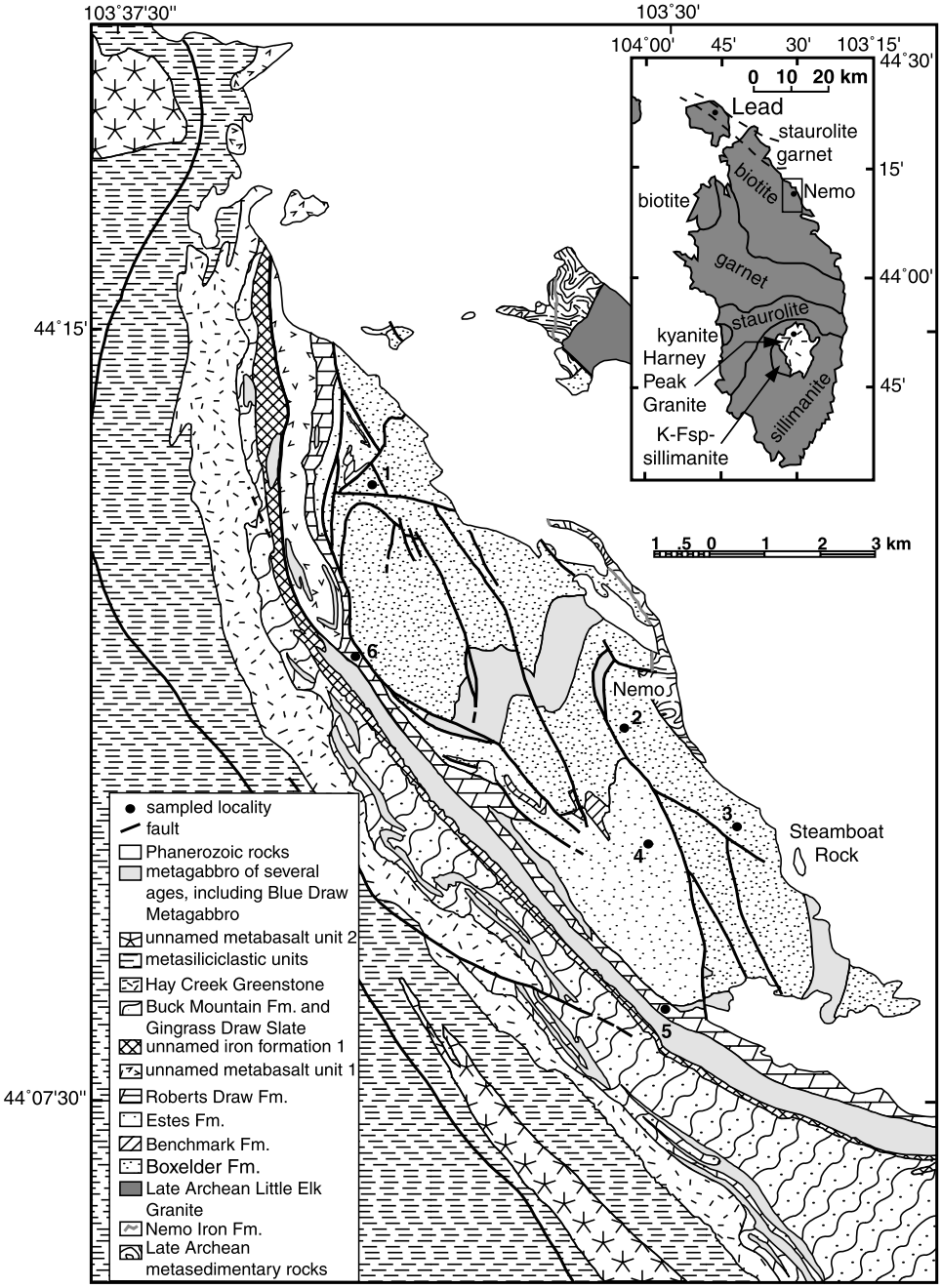

Fig. 3. Geological map of the Nemo area, Black Hills, South Dakota showing sampled localities (modified from DeWitt et al., 1986, 1989). Inset (modified from Redden et al., 1990; Dahl et al., 1999) shows metamorphic grades in the Black Hills and Harney Peak Granite. Sampled localities: Boxelder Formation: 1—Benchmark location; 2—locality near Nemo cemetery; 3—unnamed locality ~ 0.9 mile northwest from the Steamboat Rock; Estes Formation: 4—Estes Creek; Roberts Draw Formation: 5—Forest Service Rd. 201; 6—South Boxelder Creek. Carbonates from roof pendants in the Harney Peak Granite were sampled at Location 7 (shown in inset).

ginally defined from stromatolites of the Nash Fork Formation, Snowy Pass Supergroup, WY (Fenton and Fenton, 1939). On the other hand, Sims and Day (1999) proposed an Archean age for the Whalen Group based on intrusive contacts with the 2.65 Ga old Flattop Butte Granite. However, these intrusive contacts were only observed to the east from the Hartville Fault, a major N–S striking structural boundary in the Hartville uplift, whereas the thicker carbonate intervals are confined to the lower metamorphic grade western domain.

3. Analytical methods

Whole rock (marked by asterisk in Table 1) as well as microdrilled powders from the least altered portions in polished thick sections were prepared from collected samples. High metamorphic grade obliterated primary microtextures. Consequently, it was impossible to recognize and separate cements, micrites, or grains in most studied samples. Petrographic analysis reveals a lack of shear, foliation, or fracture zones. Rather, the carbonates consist of a mosaics of dolomicrospar with abundant sparry dolomite that formed during burial recrystallization. Major and trace element concentrations on whole rock samples were determined by dissolution of ~10 mg of carbonate powder in 5 ml of 0.5 M acetic acid and subsequent analysis by ICP–AES at the Geological Survey of Finland. Microdrilled powders of ~ 20–40 mg were dissolved in 5 ml of 2% nitric acid, and Mn and Sr contents were measured on a Buck Scientific 200-A AAS at Virginia Tech. Uncertainties based on the measurement of multiple standard materials by both methods were better than 5% for Sr and 10% for Mn. Samples with carbonate contents below 50% were not analyzed for major and trace elements.

Carbon dioxide was extracted at the Geological Survey of Finland from whole rock powders by closed tube reaction with anhydrous phosphoric acid ($\rho > 1.89$ g/cm^3; 16+ hours) at a temperature of 25 °C for limestone and 100 °C for dolomite, and isolated by cryogenic distillation for mass spectrometric analysis on a Finnigan MAT 251. The fractionation factors used for mineral correction of oxygen isotopes in calcite prepared at 25 °C and dolomite at 100 °C were 1.01025 and 1.00913, respectively. The external precision based on multiple standard measurements of NBS-19 was better than 0.1‰ vs. PDB for carbon and oxygen. A second generation of carbonate samples was microdrilled and the powders reacted with anhydrous phosphoric acid at 90 °C in a Micromass MultiFlow head space analyzer at the University of Maryland. The resulting carbon dioxide was delivered to a Micromass IsoPrime mass spectrometer in a stream of high-purity He. The reproducibility of carbon isotope compositions of standard materials by this technique were better than 0.1‰; however, the system was not optimized for oxygen isotope analyses, and the uncertainty on these measurements are considerably larger (ca. 1.3‰; $n = 65$). The fractionation factors used for mineral correction of oxygen isotopes in calcite and dolomite prepared at 90 °C were 1.00798 and 1.00895, respectively.

Total organic carbon (TOC) was isolated from carbonate samples by repeated acidification and centrifugation with concentrated HCl followed by washing until the sample reached neutral pH (Kaufman and Knoll, 1995). Dried samples in Vycor tubes were then mixed with CuO, evacuated, sealed, and combusted at 850 °C for 12 h. The volume of CO_2 quantified during cryogenic distillation was used to calculate organic carbon concentrations. Carbon isotope abundance in extracted and purified CO_2 was measured with a VG PRISM mass spectrometer at Mountain Mass Spectrometry. To test for the uncertainty of abundance and isotopic composition measurements on TOC, replicate ($n = 4$) analyses of organic-rich and organic-poor powders were run in the previous study (Bekker et al., 2001a). For analyses of the organic-rich sample, uncertainties were ±0.26 mg C/g for abundance (5.57 mg C/g average) and ±0.03‰ for carbon isotopic composition (−34.47‰ average); for the organic-poor sample, uncertainties were ±0.06 mg C/g (0.18 mg C/g average) and ±1.3‰ (−24.1‰ average) for abundances and carbon isotopic compositions, respectively. Two blanks analyzed in this study contained 0.74 and 1.02 μmoles of CO_2 and had

Table 1
Carbon, oxygen, and strontium isotope values and trace and major element concentrations of studied carbonates

Sample No.	Mineral/ lithology	$\delta^{13}C$, PDB	$\delta^{18}O$, PDB	TOC (mg C/g sample)	$\delta^{13}C_{TOC}$, PDB	ε_{TOC}	Ca (%)	Mg (%)	Fe (ppm)	Mn (ppm)	Sr (ppm)	Mn/Sr	$^{87}Sr/^{86}Sr$
Nash Fork Formation													
Lower part													
Massive dolomite—stromatolite (L1) member													
97-78-5	Dolomite	26.6	−7.9							1916	6	306.3	
97-78-1	Dolomite	13.7	−9.9							1561	Tr.	–	
2000-4	Dolomite	13.3	−11.5							1227	58	21.2	
2000-4/1	Dolomite	13.2	−10.0							1349	30	44.6	
2000-4/2	Dolomite	24.0	−8.4							2157	92	23.4	
2000-4/3	Dolomite	25.7	−9.1							1369	57	24.0	
2000-4/4	Dolomite	26.5	−10.4							1314	43	30.6	
2000-4/5	Dolomite	26.0	−10.5							1816	54	33.9	
2000-4/6	Dolomite	26.7	−10.1							1245	64	19.6	
2000-4/7	Dolomite	28.2	−9.3							1036	52	20	
2000-4/8	Dolomite	26.0	−10.8							1276	72	17.7	
2000-4/9	Dolomite	26.4	−9.9							1438	36	40.0	
Heterolithic siliciclastics—carbonate (L2) member													
97-3-1	Dolomite	6.1	−16.5							3040	190	16.0	
97-3-2	Dolomite	9.0	−15.5	0.1						3921	96	40.7	
97-3-3	Shale			0.2									
97-3-4	Dolomite	7.3	−6.8							1715	65	26.3	
97-3-5	Shale			0.22	−15.7								
97-3-6	Dolomite	5.1	−11.8							2279	7	316.7	
97-13-1	Dolomite	8.5	−12.7							2665	138	19.3	
97-13-2	Dolomite	8.6	−13.4							3384	178	19.0	
97-13-3	Dolomite	8.5	−14.0							1927	158	12.2	
97-13-4	Dolomite	9.0	−13.0							2511	110	22.9	
97-13-5	Dolomite	9.9	−14.4							937	Tr.	–	
97-13-6	Dolomite	8.2	−15.2	0.1	−20.6	28.4				1334	Tr.	–	
97-13-7	Dolomite	8.6	−13.7							928	Tr.	–	
118-1	Dolomite	4.8	−10.8							5059	110	46.0	
97-78-2	Dolomite	8.8	−13.1							1908	224	8.5	
97-78-3	Dolomite	6.1	−14.8							563	Tr.	–	
97-78-4	Dolomite	8.9	−13.7							2320	236	9.8	
BE-C-95-17*	Dolomite	4.8	−17.2				23.13	12.56	18867	4252	206	20.7	
BE-C-95-18*	Dolomite	6.8	−15.9				21.94	12.69	3284	1122	140	8.0	
WY-96-35*	Dolomite	7.0	−14.3				23.09	11.88	36883	2848	265	10.8	
WY-96-36	Dolomite	7.7	−11.4							704	107	6.6	
WY-96-37	Dolomite	7.1	−11.0							1249	77	16.1	
WY-96-24	Dolomite	7.2	−12.7							959	112	8.6	

Table 1 (*Continued*)

Sample No.	Mineral/ lithology	$\delta^{13}C$, PDB	$\delta^{18}O$, PDB	TOC (mg C/g sample)	$\delta^{13}C_{TOC}$, PDB	ε_{TOC}	Ca (%)	Mg (%)	Fe (ppm)	Mn (ppm)	Sr (ppm)	Mn/Sr	$^{87}Sr/^{86}Sr$
WY-96-25*	Dolomite	7.4	−12.8				23.05	12.46	22942	2371	196	12.1	
97-116A	Dolomite	7.0	−8.2							322	15	20.8	
97-9-1	Dolomite	8.0	−10.6							1188	64	18.4	
97-9-2	Dolomite	7.1	−9.6							849	5	161.9	
2000-20	Dolomite	8.6	−15.7							1769	194	9.1	
Silicified dolomite with large domal digitate stromatolites (L3) member													
97-20-1	Dolomite	6.6	−9.3							958	20	46.9	
2000-18	Dolomite	7.3	−9.5							449	135	3.3	
Nodular dolomite (L4) member													
97-56-2	Dolomite	7.0	−9.8							367	140	2.6	
WY-96-23*	Dolomite	6.9	−11.1				22.72	13.21	7197	1074	104	10.4	
WY-96-26	Dolomite	8.3	−8.8							167	121	1.4	
WY-96-27*	Dolomite	8.2	−8.8				22.82	13.59	4541	623	249	2.5	0.704947
2000-16	Dolomite	5.3	−10.0							1327	51	26.1	
2000-17	Dolomite	7.1	−10.7							872	113	7.7	
97-56-1	Argillite			0.1									
2000-19	Dolomite	8.0	−10.9							107	190	0.6	
Silicified dolomite with large domal digitate stromatolites (L5) member													
WY-96-33*	Dolomite	6.4	−10.6				22.63	12.97	9005	1173	95	12.4	
Nodular dolomite (L6) member													
WY-96-22	Dolomite	7.5	−9.7							240	97	2.5	
WY-96-38	Dolomite	7.5	−9.6							330	20	16.8	
WY-96-39	Dolomite	7.5	−8.6							582	192	3.0	
97-65-1	Dolomite	6.3	−8.5							438	54	8.1	
2000-10/1	Dolomite	7.3	−8.7							440	190	2.3	
2000-11/1	Dolomite	8.2	−7.1							185	148	1.3	
2000-12/1	Dolomite	7.2	−8.7							456	32	14.2	
2000-13/1	Dolomite	6.3	−9.5							1345	77	17.4	
2000-14	Dolomite	6.6	−8.8							750	134	5.6	
2000-15	Dolomite	7.1	−8.7							434	156	2.8	
Heterolithic siliciclastics—carbonate (L7) member													
WY-96-20*	Dolomite	8.1	−8.6				23.19	13.85	1884	382	72	5.3	
WY-96-32*	Dolomite	6.4	−11.9				22.95	13.75	5876	826	112	7.4	
BE-C-95-19*	Dolomite	8.2	−10.1				21.81	12.66	3389	391	234	1.7	
WY-96-21	Dolomite	7.5	−11.4							520	131	4.0	
97-66-1	Dolomite	6.2	−12.1							416	114	3.6	
97-66-2	Dolomite	6.9	−10.6							952	186	5.1	
Stromatolitic dolomite (L8) member													

Table 1 (*Continued*)

Sample No.	Mineral/ lithology	$\delta^{13}C$, PDB	$\delta^{18}O$, PDB	TOC (mg C/g sample)	$\delta^{13}C_{TOC}$, PDB	ε_{TOC}	Ca (%)	Mg (%)	Fe (ppm)	Mn (ppm)	Sr (ppm)	Mn/Sr	$^{87}Sr/^{86}Sr$
97-23-1	Dolomite	6.7	−8.0							643	20	32.9	
97-23-2	Dolomite	5.5	−6.6							1391	63	22.2	
97-41-1	Dolomite	5.9	−7.6							712	38	19.0	
WY-96-13*	Dolomite	5.6	−12.2				21.77	12.46	19988	1566	161	9.7	
WY-96-14	Dolomite	6.5	−11.5							251	159	1.6	
WY-96-15*	Dolomite	6.0	−11.1				22.38	12.88	10890	710	172	4.1	
WY-96-16	Dolomite	4.7	−11.0							382	98	3.9	
WY-96-17	Dolomite	4.5	−9.5							384	176	2.2	
WY-96-19	Dolomite	5.4	−10.8							885	88	10.0	
WY-96-31	Dolomite	6.2	−10.7							583	161	3.6	
97-5-1	Dolomite	6.2	−8.2							407	101	4.0	
97-7-1	Dolomite	6.1	−8.4							678	153	4.4	
97-7-2	Dolomite	5.6	−7.7							512	100	5.1	
97-7-3	Dolomite	5.6	−6.8							726	63	11.5	
97-7-4	Shale			1.3	−16.2								
97-8-1	Dolomite	6.1	−6.7							281	239	1.2	
97-8-2str	Dolomite	5.7	−8.9							155	107	1.5	
97-8-2l	Dolomite	7.0	−5.6							151	80	1.9	
97-8-2d	Dolomite	6.4	−7.5							545	117	4.6	
Lower part, undivided													
WY-96-1*	Dolomite	7.1	−10.3				22.72	13.19	8686	1610	121	13.3	
WY-96-1a	Dolomite	3.9	−12.3							338	133	2.5	
WY-96-2/1*	Dolomite	5.2	−14.1				21.70	12.54	9378	2110	177	11.9	
WY-96-2/2*	Dolomite	5.0	−14.4				22.39	12.38	10000	2223	185	12	
97-11-1	Dolomite	8.1	−6.4							204	Tr.	–	
97-12-1	Dolomite	7.2	−5.8							610	Tr.	–	
Lower carbonaceous shale (M1) member													
97-6-1	Shale			6.2	−17.4								
97-39-1	Shale			26.8	−21.9								
97-40-1	Shale			27.3	−30.8								
97-42-1	Shale			98.3	−23.0								
97-43-2	Dolomite	5.5	−8.8							758	Tr.	–	
97-64-1	Shale			4.3	−6.9								
97-67-1	Shale			3.0	−9.8								
Heterolithic siliciclastics-nodular dolomite (M2) member													
97-74-1	Dolomite	7.6	−6.1							650	206	3.1	
97-37-1	Dolomite	7.7	−9.1							298	165	1.8	
97-46-2	Dolomite	6.3	−11.7							2180	145	15.0	
WY-96-40*	Dolomite	7.9	−9.8				23.1	13.56	3727	358	234	1.5	

Table 1 (*Continued*)

Sample No.	Mineral/ lithology	$\delta^{13}C$, PDB	$\delta^{18}O$, PDB	TOC (mg C/g sample)	$\delta^{13}C_{TOC}$, PDB	ε_{TOC}	Ca (%)	Mg (%)	Fe (ppm)	Mn (ppm)	Sr (ppm)	Mn/Sr	$^{87}Sr/^{86}Sr$
WY-96-43	Dolomite	7.0	−7.8							1106	60	18.4	
WY-96-8	Dolomite	6.6	−8.1							82	221	0.4	
97-63-1	Dolomite	5.8	−10.1							1013	70	14.5	
2000-8	Dolomite	6.2	−11.3							518	162	3.2	
2000-9/1	Dolomite	7.4	−9.6							84	16	5.2	
2000-9/2	Dolomite	7.6	−8.7							158	130	1.2	
2000-10	Dolomite	7.0	−13.9							393	150	2.6	
2000-11	Dolomite	7.2	−7.9							429	172	2.5	
2000-12	Dolomite	7.1	−9.1							240	135	1.8	
2000-13	Dolomite	5.5	−11.2							1159	145	8.0	
WY-96-10*	Dolomite	3.1	−14.5				22.42	13.14	11159	590	293	2	0.714247
Upper carbonaceous shale (M3) member													
WY-96-9	Shale			4.6									
97-73-1	Shale			3.5	−15.8								
97-15-1	Shale			9.4	−19.2								
97-46-1	Shale			4.1	−15.7								
97-46-3	Shale			12.0	−22.2								
97-51-1	Schist			0.01	−16.5								
97-54-1	Shale			121.8	−17.7								
97-54-2	Dolomite	2.0	−6.8							396	51	7.8	
97-54-3a	Dolomite	2.4	−6.8							79	tr.	–	
97-54-3b	Dolomite	2.4	−6.6							235	1	308	
97-60-1	Shale			5.9	−28.2								
97-63a-1	Shale			203.6	−22.3								
97-105-1	Shale			2.4	−21.9								
Massive dolomite (U1) member													
Lower part													
WY-96-11*	Dolomite	2.5	−8.9				22.91	13.69	1167	192	54	3.6	
WY-96-28*	Dolomite	2.2	−9.0				23.14	13.89	1445	230	54	4.3	
WY-96-45	Dolomite	2.4	−7.2							78	15	5.2	
97-29-1	Dolomite	2.5	−6.0							168	10	16.6	
97-29-2	Dolomite	2.5	−6.2							68	Tr.	–	
97-52-1	Dolomite	2.4	−3.5							342	Tr.	–	
97-45-1	Dolomite	1.9	−7.9							496	29	17.1	
97-45-2	Dolomite	2.4	−6.6							105	1	143.8	
97-120-1	Dolomite	1.9	−9.3							403	7	54.4	
WY-96-29*	Dolomite	0.7	−13.1				22.6	13.39	7514	695	132	5.3	
WY-96-41*	Dolomite	2.4	−9.2				23.09	13.76	2711	552	42	13.2	
97-30-1	Dolomite	2.5	−7.6							402	Tr.	–	
WY-96-44*	Dolomite	1.5	−7.9				23.17	13.05	2495	199	55	3.6	

Table 1 (*Continued*)

Sample No.	Mineral/ lithology	$\delta^{13}C$, PDB	$\delta^{18}O$, PDB	TOC (mg C/g sample)	$\delta^{13}C_{TOC}$, PDB	ε_{TOC}	Ca (%)	Mg (%)	Fe (ppm)	Mn (ppm)	Sr (ppm)	Mn/Sr	$^{87}Sr/^{86}Sr$
97-34-1	Dolomite	1.1	−17.4							364	3	121.7	
2000-1A	Dolomite	0.1	−9.3							321	72	4.5	
2000-1B	Dolomite	−0.2	−10.8										
Upper part													
WY-96-12-1	Dolomite	2.5	−8.6							389	17	22.3	
WY-96-12-2	Dolomite	1.0	−4.8							376	17	21.6	
97-31-1	Dolomite	1.1	−5.3							514	13	40.0	
2000-3	Dolomite	1.5	−4.8							84	47	1.8	
WY-96-3*	Dolomite	1.3	−9.0				22.33	13.34	3277	425	32	13.4	
WY-96-4	Dolomite	1.6	−5.6							116	35	3.3	
97-2-1	Dolomite	0.2	−10.7							373	159	2.4	
97-2-2	Dolomite	0.8	−8.8							364	30	12.3	
97-2-3	Dolomite	0.6	−5.4							172	21	8.2	
97-2-4	Dolomite	0.6	−6.6							268	73	3.7	
97-14-1	Dolomite	0.3	−5.0							392	17	22.8	
97-14-2	Dolomite	1.1	−4.5							256	45	5.7	
BE-C-95-5*	Dolomite	0.2	−7.4	0.1	−19.6	19.8	22.87	13.36	1564	253	83	3.1	
97-32-1	Dolomite	0.5	−7.2							1773	1	2317	
97-33-4	Dolomite	0.1	−9.1							613	12	49.8	
2000-6	Dolomite	1.2	−8.2							207	46	4.5	
WY-96-5*	Dolomite	1.9	−8.7				22.69	13.58	2454	159	34	4.7	
WY-96-6*	Dolomite	1.4	−7.4				23.06	13.39	7811	404	69	5.9	
2000.2.2	Argillite			0.1									
Slaughterhouse Formation, Sierra Madre													
97-SL-1*	Dolomite	8.0	−10.4						228	32	7.1		
97-SL-1/2*	Dolomite	6.6	−11.6						280	33	8.5		
97-SL-3*	Dolomite	5.9	−14.6						780	77	10.2		
97-SL-4*	Dolomite	7.8	−12.7						1101	65	17.0		
97-SL-5	Phyllite			19.3	−22.6								
97-SL-6*	Dolomite	8.7	−10.8						430	43	9.9		
97-SL-7*	Dolomite	7.3	−11.1						324	39	8.3		
97-SL-8*	Dolomite	16.6	−10.3						1469	153	9.6		
97-SL-9*	Dolomite	15.2	−4.2						1842	15	119.9		
Whalen Group, Hartville Uplift													
Locality 1													
2HV-26	Dolomite	1.0	-7.4						46	17	2.7		
2HV-27	Dolomite	0.9	−8.9						55	21	2.6		
2HV-28	Dolomite	0.9	−9.0						51	17	3.0		

Table 1 (*Continued*)

Sample No.	Mineral/ lithology	$\delta^{13}C$, PDB	$\delta^{18}O$, PDB	TOC (mg C/g sample)	$\delta^{13}C_{TOC}$, PDB	ε_{TOC}	Ca (%)	Mg (%)	Fe (ppm)	Mn (ppm)	Sr (ppm)	Mn/Sr	$^{87}Sr/^{86}Sr$
Locality 2													
HV-2-1*	Dolomite	1.1	−6.5			21.38	13.02	988	62	50	1.2		
HV-2-4*	Dolomite	1.4	−7.3			22.39	13.31	6381	462	32	14.3		
Locality 3													
HV-96-1	Dolomite	0.8	−5.2						98	Tr.	–		
HV-96-2	Dolomite	−0.3	−4.2						97	25	3.8		
HV-96-3	Dolomite	1.0	−5.2						84	9	9.6		
Locality 4													
2HV-29	Dolomite	0.9	−4.9						35	56	0.6		
Locality 5													
HV-4-2*	Dolomite	1.1	−8.4			22.06	12.96	1201	70	38	1.9		
Locality 6													
HV-5-1	Dolomite	0.7	−6.3						499	35	14.4		
Locality 7													
HV-9-1*	Mixture	1.3	−9.0			26.61	11.04	2138	234	38	6.1		
HV-9-1*	Dolomite	2.1	−7.0										
2HV-24	Dolomite	1.2	−5.8						59	53	1.1		
2HV-25	Dolomite	3.2	−5.6						169	53	3.2		
Locality 8													
HV-13-1	Dolomite	6.3	−5.9						955	21	46.0		
2HV-14	Dolomite	2.8	−15.0						2755	83	33.0		
2HV16	Dolomite	7.3	−13.2						1762	95	18.6		
2HV-17	Dolomite	5.9	−12.0						961	41	23.3		
2HV-18	Dolomite	5.6	−9.5						602	57	10.6		
2HV-19	Dolomite	8.2	−8.0						125	125	1.0		
2HV21	Dolomite	4.5	−13.7						730	78	9.4		
2HV-22	Dolomite	5.4	−8.8						612	68	9.1		
2HV-23	Dolomite	8.0	−8.2						374	122	3.1		
2HV-24-1	Dolomite	4.8	−9.6						1478	51	29.2		
Locality 9													
2HV-1	Dolomite	0.1	−11.1						1068	71	15.1		
2HV-2	Dolomite	5.2	−13.0						956	87	11.0		
2HV-3	Dolomite	6.9	−11.6						481	89	5.4		
2HV-4	Dolomite	5.6	−11.4						734	72	10.3		
2HV-5	Dolomite	6.2	−9.5						386	108	3.6		
Locality 10													
2HV-6	Dolomite	2.0	−12.6						2301	36	64.1		
2HV-8	Dolomite	3.7	−13.7						3286	118	27.8		

Table 1 (*Continued*)

Sample No.	Mineral/ lithology	$\delta^{13}C$, PDB	$\delta^{18}O$, PDB	TOC (mg C/g sample)	$\delta^{13}C_{TOC}$, PDB	ε_{TOC}	Ca (%)	Mg (%)	Fe (ppm)	Mn (ppm)	Sr (ppm)	Mn/Sr	$^{87}Sr/^{86}Sr$
Locality 11													
2HV-9	Dolomite	0.5	−7.7						330	31	10.7		
2HV-9-1	Dolomite	0.3	−6.7						363	47	7.8		
2HV-10	Dolomite	−0.3	−7.9						38	115	0.3		
2HV-11	Dolomite	0.4	−10.0						84	48	1.8		
2HV-12	Dolomite	0.5	−6.5						216	60	3.6		
Locality 12													
2HV-20	Dolomite	7.9	−9.8						311	136	2.3		
Black Hills, SD													
Boxelder Formation													
B99.1	Dolomite	1.0	−10.7						3236	Tr.	–		
B99.2	Dolomite	0.7	−9.6						2866	Tr.	–		
B99.3	Dolomite	0.7	−20.8						3863	Tr.	–		
B99.3	Dolomite	0.8	−10.8										
B99.4	Dolomite	1.0	−11.1						4698	Tr.	–		
B99.5	Dolomite	0.5	−12.1						3391	Tr.	–		
B99.6	Dolomite	1.1	−11.8						3368	Tr.	–		
B99.7l	Dolomite	−0.7	−18.8						5040	Tr.	–		
B99.7d	Dolomite	−1.4	−12.0						5961	Tr.	–		
B99.8	Dolomite	−0.1	−13.4						9401	Tr.	–		
SD-96-6*	Dolomite	−1.1	−17.6										
SD-96-6*	Mixture	−1.3	−17.7			27.4	8.7	27430	10919	214	50.9		
SD-96-6*	Calcite	−1.8	−17.1										
SD-96-9*	Dolomite	−0.7	−16.3			23.0	12.8	10297	7121	45	157		
SD-96-13	Dolomite	−0.8	−13.2						6939	29	235.7		
Estes Creek Formation													
SD99.2.1	Dolomite	1.3	−14.0						6776	5	1339		
SD99.2.1	Dolomite	1.4	−13.5										
SD99.2.2	Dolomite	2.2	−16.8						537	Tr.	–		
SD99.2.2	Dolomite	2.3	−13.9										
SD99.2.3	Dolomite	2.1	−12.7						1382	17	82.1		
SD99.2.4	Dolomite	2.1	−14.3						909	7	125.4		
SD99.2.5	Dolomite	2.0	−13.2						1891	Tr.	–		
SD99.2.6	Dolomite	2.3	−14.2						1009	Tr.	–		
SD99.2.7	Dolomite	2.4	−11.7						729	6	127.2		
SD99.2.8	Dolomite	2.2	−14.7						12118	Tr.	–		
SD99.2.9	Dolomite	2.5	−14.4						515	Tr.	–		
SD99.2.10	Dolomite	2.4	−6.2						638	Tr.	–		

Table 1 (*Continued*)

Sample No.	Mineral/ lithology	$\delta^{13}C$, PDB	$\delta^{18}O$, PDB	TOC (mg C/g sample)	$\delta^{13}C_{TOC}$, PDB	ε_{TOC}	Ca (%)	Mg (%)	Fe (ppm)	Mn (ppm)	Sr (ppm)	Mn/Sr	$^{87}Sr/^{86}Sr$
Roberts Draw Formation													
B99.10	Dolomite	−0.4	−13.6						597	25	24.4		
B99.11d	Dolomite	1.3	−9.7						394	Tr.	–		
B99.11l	Dolomite	1.6	−8.1						444	2	201.3		
B99.12	Dolomite	1.2	−10.7						814	Tr.	–		
B99.13	Dolomite	1.9	−7.3						828	Tr.	–		
B99.14	Calcite	−0.2	−9.8						694	Tr.	–		
B99.14	Calcite	−0.2	−9.0										
B99.15	Calcite	−1.1	−10.1						2720	Tr.	–		
B99.16	Calcite	0.0	−11.0						871	Tr.	–		
SD-96-4*	Dolomite	−3.5	−15.6			22.87	12.8	13083	1075	106	10.1		
SD-96-1*	Dolomite	1.1	−17.3			21.8	12.4	8961	2626	149	17.6		
Marble from roof complex (country rock), Harney Peak Granite area, Black Hills, SD													
HP-1	Dolomite	2.1	−8.1						282	45	6.3		
HP-2	Dolomite	2.2	−6.0						103	57	1.8		
HP-3	Dolomite	2.3	−5.4						161	28	5.8		

carbon isotope values −20.28 and −20.27‰, respectively.

Samples chosen for Sr isotopic analysis were treated repeatedly with 0.4 M ammonium acetate (three times; pH 8.2) prior to dissolution with 0.5 M acetic acid in order to remove diagenetic components (Gorokhov et al., 1995; Montañez et al., 1996). Strontium was eluted from solution by ion exchange chromatography using ElChrom Sr spec resin and weak 0.05 M nitric acid and measured on a VG Sector 54 multicollector thermal ionization mass spectrometer at the University of Maryland. Repeated analysis of NBS-987 over a period of 3 months gave a value of 0.710248 ± 0.000005.

4. Nash Fork Formation

4.1. Description

The Nash Fork Formation is the lowermost unit in the upper Libby Creek Group and has a thickness of ~1.7 km. It is exposed in the core of a steeply, south-dipping homocline in the central part of the Medicine Bow Mountains (Karlstrom and Houston, 1984). The lower contact is structural along the Lewis Lake Fault and the upper contact is not exposed but is considered to be comformable with the Towner Greenstone (Fig. 2). The results of detailed sedimentological studies of the Nash Fork Formation are presented in Bekker and Eriksson (in press) and only a short summary will be given here. The Nash Fork Formation is separated by two carbonaceous shales, interpreted as drowning events into lower, middle, and upper units. The formation is further subdivided into 12 distinct members based on detailed mapping in an area between the Small Telephone Lake and Prospector Lake, about 2.2 km along strike (Fig. 4).

The lower Nash Fork Formation consists of interlayered massive and stromatolitic dolomite facies associations, heterolithic siliciclastics–carbonate facies associations, silicified domal digitate stromatolite, and nodular dolomite facies associations (Fig. 5). The L1 member consists of massive and stromatolitic dolomite facies association with tufa structures and small domal stromatolites with radial structures (Fig. 6) suggesting deposition in an upper intertidal to supratidal setting. Heterolithic siliciclastics–carbonate facies associations (the L2, L7, and lower L8 members; Fig. 5) represent peritidal deposition. This facies association contains upward-shallowing parasequences of gray or brown dolomite, dolosiltite, and argillite occasionally capped by sandstone. Ubiquitous sulfate molds in argillites and dolomites suggest an arid depositional environment. Nodular dolomite facies associations (the L4 and L6 members; Fig. 5) consist of parasequences containing from the base to the top of gray dolomite, dolomite with silicified nodules, brown dolomite, and argillite; these are interpreted as inner shelf to supratidal deposits. Domal digitate stromatolite facies associations (the L3, L5, and upper L8 members; Fig. 5) consist predominantly of silicified domal digitate stromatolites with thin parted and ribbon dolomite facies at the base and gray dolomite at the top. This facies association likely developed during flooding of the carbonate platform.

The middle Nash Fork Formation consists of three members and includes carbonaceous shales and heterolithic siliciclastics–nodular dolomite facies associations. Carbonaceous shale facies associations (M1 and M3 members) consist of upward-coarsening parasequences of black organic-rich shale with pyrite, siltstone, and sandstone with thin beds of brown dolomite and black shale, and likely developed in response to platform drowning. Heterolithic siliciclastics–nodular dolomite facies associations of the M2 member consist of upward-shallowing parasequences of gray dolomite, dolomite with silicified nodules, brown dolomite and siltstone with sulfate molds that record inner shelf to supratidal depositional conditions.

The upper Nash Fork Formation above the upper carbonaceous shale (M3 member) consists of a massive dolomite facies association (U1 member) and contains a prominent karstic surface overlain by fluvial quartzite dividing the member into two parts (Fig. 5). This facies association consists of upward-shallowing parasequences of organic-rich dolomite, gray dolomite, dolosiltite,

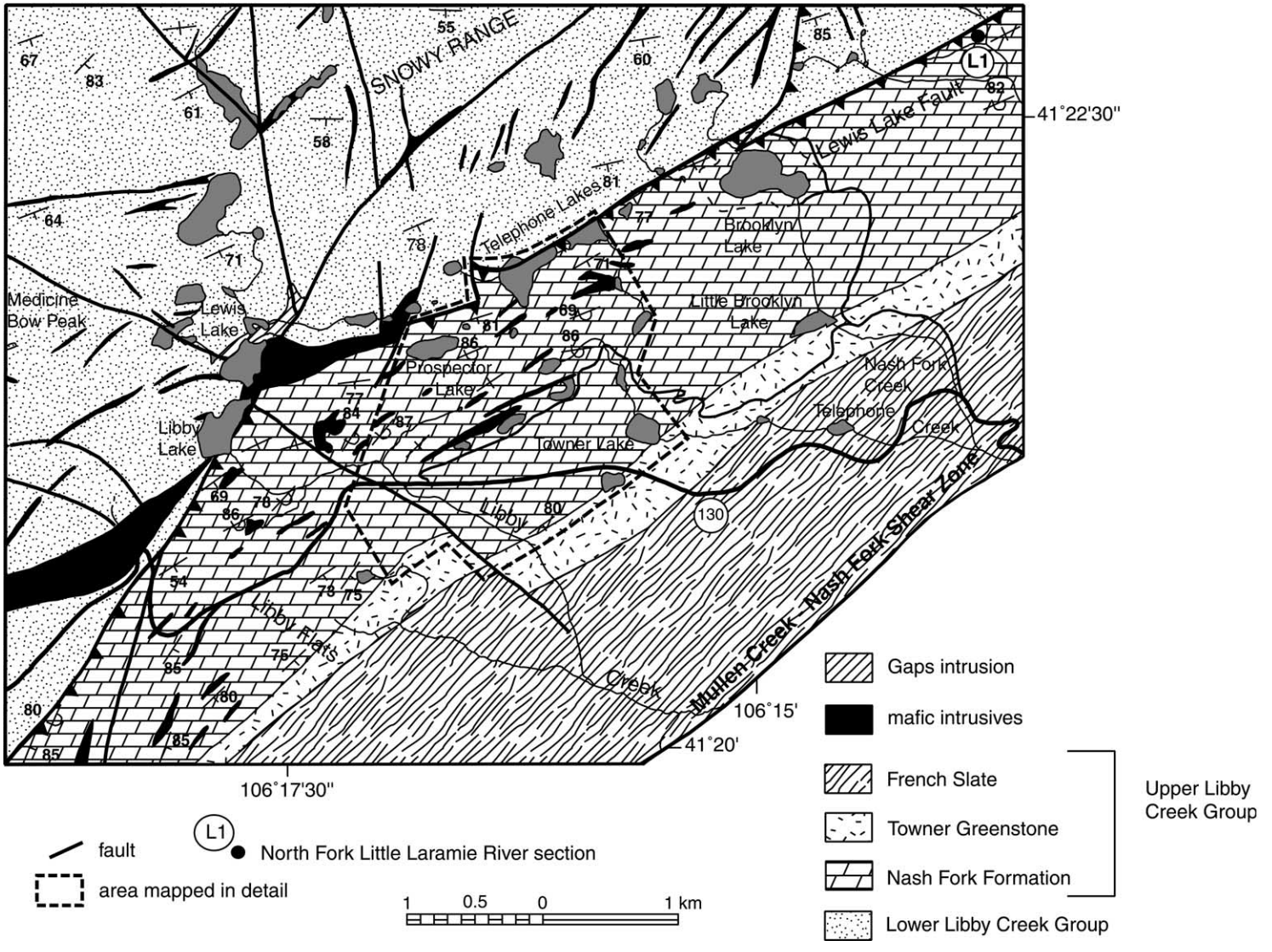

Fig. 4. Detailed map of the Nash Fork Formation in the area between the Small Telephone Lake and Libby Creek in the Medicine Bow Peak Quadrangle.

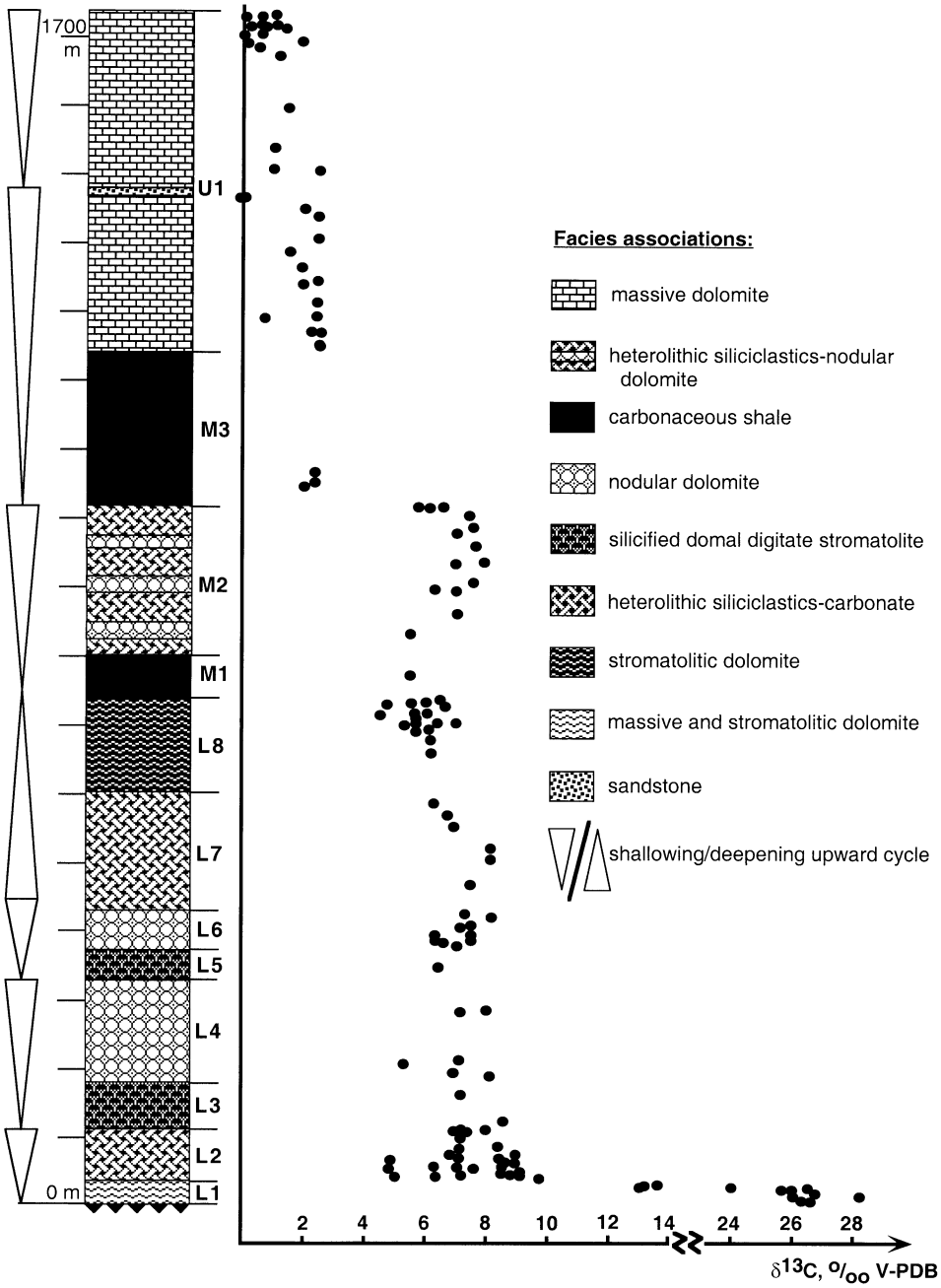

Fig. 5. Stratigraphic column, inferred cycles and variations of $\delta^{13}C_{carb}$ values in the Nash Fork Formation.

and brown dolomite that reflects deposition in outer shelf to subaerial environments.

There is no evidence for a restricted depositional environment in any of the 12 members of the Nash Fork Formation in the form of such features as bedded evaporites. Rather, the presence of facies indicative of tidal flat, lagoonal, inner and outer shelf, and drowned platform environments and the

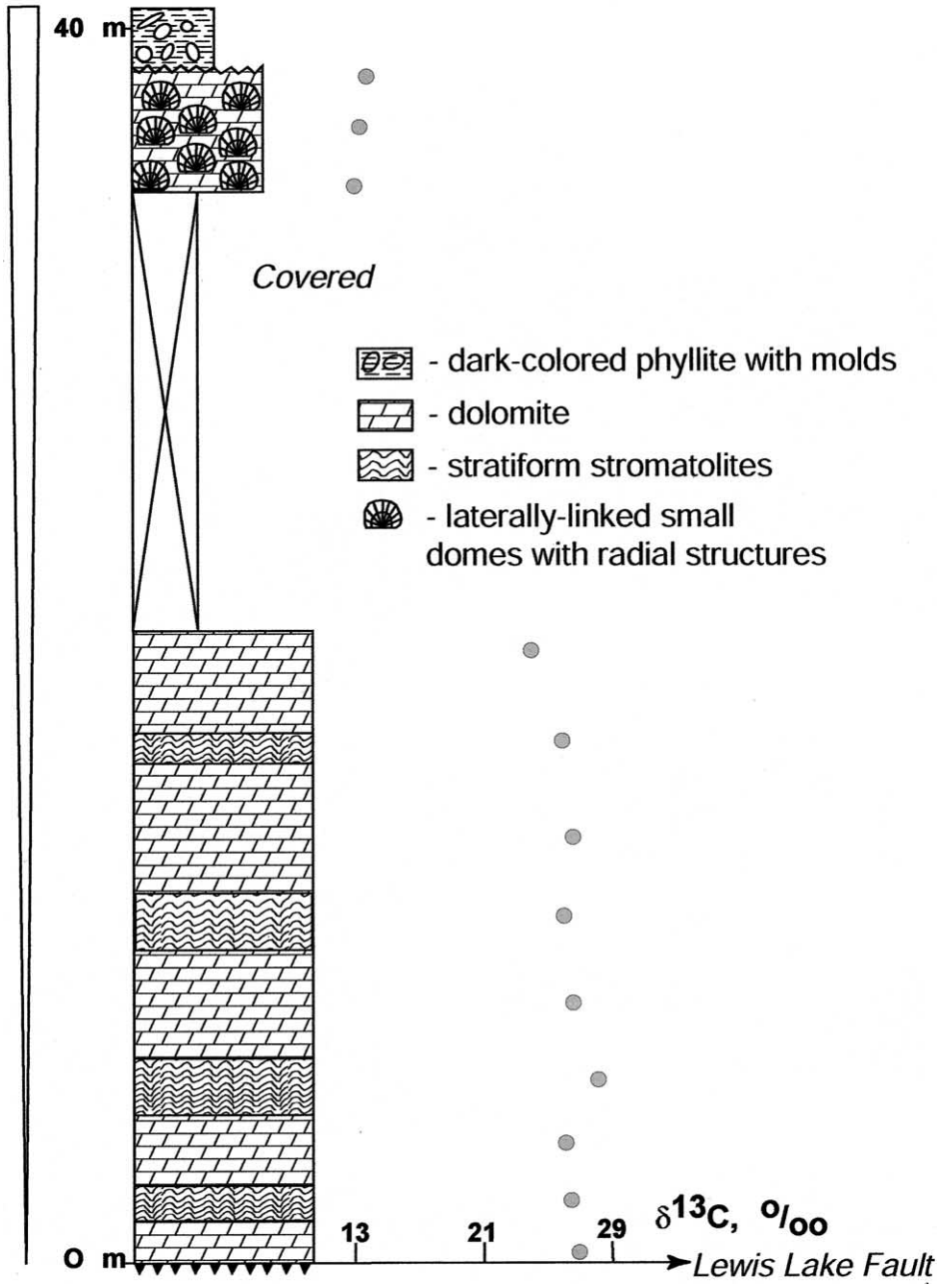

Fig. 6. Stratigraphic column and variations of $\delta^{13}C$ values in the basal dolomite member (L1) in the North Fork of the Little Laramie River.

sequence architecture (Bekker and Eriksson, in press) suggest that the Nash Fork Formation developed entirely in open-marine settings on a mature passive margin along the southern edge of the Wyoming Craton. Facies associations in the lower Nash Fork Formation are most compatible with a low-energy, low-gradient protected platform. Two drowning events in the middle part of the Nash Fork modified the depositional profile of the platform. Drowning caused a shutdown of carbonate production and changed the depositional profile from the low-energy, low-gradient protected platform to an unprotected shelf with a higher gradient for the middle and upper Nash Fork Formation.

Samples for this study were collected in the area mapped in detail (Fig. 4). Wherever possible, detailed sections of members were measured and samples were collected within this framework. However, for some members, poor outcrop did not permit section measuring and collected samples were tied to a generalized stratigraphic section (Fig. 5) by their position with respect to the top or the bottom of these members. In addition, samples were collected in several places within the mapped area to test variability within members. In sum, all samples are confidently assigned to members.

4.2. Geochemical data and diagenesis

Results of geochemical analyses of closely spaced Nash Fork Formation samples are provided in Table 1. All samples are dolomite, but they have highly variable Mn (68–5,059 ppm), Fe (1167–36,883 ppm) and Sr (tr.–293 ppm) contents. Oxygen isotope values also vary widely, ranging between −17.4 and −3.5‰ (V-PDB), but most samples have $\delta^{18}O$ values above −14‰. The most enriched ^{18}O values are consistent with those found in well-preserved Paleoproterozoic and Mesoproterozoic carbonate successions (Burdett et al., 1990; Veizer et al., 1992a,b; Buick et al., 1995; Melezhik et al., 1997b; Kah, 2000; Frank and Lyons, 2000; Lindsay and Brasier, 2000, 2002; Bekker et al., 2001a). Notably, the $\delta^{18}O$ composition of samples from the upper Nash Fork Formation dolomites are higher than those for the lower part of the formation, which has more diverse lithologies and was likely stronger affected by postdepositional changes. The overall low $\delta^{18}O$ values of these samples are consistent with the general high grade of metamorphism these rocks experienced during recrystallization, although some samples appear to have been little altered. The low TOC contents (ca. 0.1 mg C/g sample) and highly variable fractionation between organic and carbonate carbon (19.8–28.6‰) in these dolomites are also consistent with the metamorphic grade. As expected, shales have generally higher organic carbon contents, up to 203.6 mg C/g sample (most samples contained more than 3 mg C/g sample), but equally variable carbon isotope compositions (Table 1). All these indicators suggest that caution should be taken when interpreting temporal variations in the carbon isotopic composition of carbonate, although the low degree of variability of $\delta^{13}C$ within discrete members suggests that secondary insults had little effect in this rock-dominated system.

Based on carbonate analyses, strong temporal trends in $\delta^{13}C$ are noted in the Nash Fork Formation. Most notably, the lower 20 m of the L1 member (Fig. 6) have the highest carbon isotope values (between +24 and +28.2‰) ever reported from marine carbonates. These are followed upsection by a rapid decrease to +13‰ near the top of the member. For the remainder of the lower and middle Nash Fork Formation (L2 to M2 members), carbon isotope values remain in +6 to +8‰ range (Fig. 5). Oxygen isotopes in the same suite of samples hover around −10‰, suggesting neither excessive alteration nor primary evaporitic conditions, although manganese concentrations are unusually high in the lower two members of the formation. Carbonate samples from overlying heterolithic members have generally lighter and more variable $\delta^{18}O$ compositions than massive dolomites. This trend changes in the M3 member and overlying carbonates of the U1 member, which have $\delta^{13}C$ values between 0 and +2.5‰. If this trend is primary, the Nash Fork Formation preserves a remarkable shift in carbon isotope values of over 25‰.

Two samples with low Mn/Sr values were analyzed for Sr isotope ratios. Sample WY-96-27 from the lower Nash Fork Formation has a

Table 2
Paleoproterozoic succession containing carbonates with $\delta^{13}C_{carb}$ values > +8‰

Name of unit	Location	Age constraints	$\delta^{13}C_{max}$ values (‰)	Reference
Dunphy, Uvé and Alder Fms.	Labrador Trough, Canada	2169–2142 Ma	15.4	Melezhik et al., 1997a
Juderina Fm.	Nabberu Province, Australia	ca. 2173 Ma	9.4	El Tabakh et al., 1999; Lindsay and Brasier, 2002; our unpubl. data
Aravalli Supergroup	India	1900–2200 Ma	11.1	Sreenivas et al., 2001; our unpubl. data
Unnamed marble unit	Lofoten-Vesterålen, Norway	Early PR_1	12.1	Baker and Fallick, 1989a
Loch Maree Gr.	Scotland	Early PR_1	12.9	Baker and Fallick, 1989b
Nash Fork Fm.	Wyoming, USA	Early PR_1	28.2	This paper
Slaughterhouse Fm.	Wyoming, USA	Early PR_1	16.6	This paper
Lomagundi and Deweras Grs.	Zimbabwe	Early PR_1 (>2.0 Ga)	16.3	Bekker et al., 2001b
Mako Supergroup	Eastern Senegal	ca. 2.15 Ga	~10	Master et al., unpubl.
Silverton and Lucknow Fms.	South Africa	Early PR_1 (>2061 Ma)	11.3	Master et al., 1993; Buick et al., 1998; Swart, 1999; Bekker et al., 2001a
Peribonca Fm.	Otish Basin, Que., Canada	Early PR_1	10.3	Our unpubl. data
Kona Dolomite	MI, USA	Early PR_1	9.5	Our unpubl. data
Carbonate unit from the Hurwitz Group	Quartzite Lake, Nunavut, Canada	Early PR_1 (>2.11 Ga)	9.1	Hofmann and Davidson, 1998; our unpubl. data
Paso Severino Fm.	San Jose Belt, Uruguay	2145–2074 Ma	11.6	Our unpubl. data
Jatulian carbonates	Finland; Karelia and Kola Peninsula, Russia	2.2–2.1 Ga	18.0	Yudovich et al., 1990; Karhu, 1993; Melezhik and Fallick, 1996; Melezhik et al., 1999a
Yakovlevskaya Suite	Voronezh Massif, Russia	Early PR_1	11.7	Akhmedov et al., 1996

$^{87}Sr/^{86}Sr$ isotope ratio of 0.704947 that is comparable although slightly higher than the lowest Sr isotope values (~0.7035) measured from likely correlative successions in Fennoscandia and Zimbabwe (Master et al., 1990; Gorokhov et al., 1998). Sample WY-96-10 from the middle part of the Nash Fork Formation has a very high $^{87}Sr/^{86}Sr$ isotope ratio (0.714247) and that value is not considered to be primary. High Fe content and low oxygen and carbon isotope values of this sample support significant alteration.

4.3. Speculations on the origin of extraordinary ^{13}C-enrichment

The highly enriched carbon isotope values in the L1 member of the Nash Fork Formation have no match in Earth history, although $\delta^{13}C$ values above +10‰ and as high as +18‰ are common in Paleoproterozoic (Table 2) and Neoproterozoic (up to +12‰; cf. Kaufman and Knoll, 1995) carbonate successions worldwide. These extreme values might be produced locally by high degrees of seawater evaporation (Stiller et al., 1985; see for contrary view, Lazar and Erez, 1990) or methanogenesis (Reitsema, 1980; Talbot and Kelts, 1986), but are hard to reconcile with open marine conditions. Melezhik et al. (1999a) attributed values as high as +18‰ in Paleoproterozoic dolomite succession from Karelia, Russia, to high stromatolite productivity.

We relate the extreme ^{13}C-enrichment in the L1 member to basinwide and, likely, global rather than local processes for the following reasons: (1) a

lack of evidence for evaporites and accompanying ^{18}O enrichment; (2) stromatolites are less common in this member than in other members; (3) a stratigraphically consistent trend of $\delta^{13}C$ values, lack of variation in $\delta^{13}C$ values on a sample scale, shallow-water environment of deposition, and lack of associated organic-rich lithologies argues against local methanogenesis as a sole source of this signal.

The fraction of carbon buried as organic matter (f_{org}) can be calculated based on the rearranged carbon isotope mass balance equation (cf. Hayes et al., 1999): $f_{org} = (\delta_{carb} - \delta_i)/\varepsilon_{TOC}$, where δ_{carb} and δ_i are the isotopic compositions of carbonates and total carbon input to the surface environment, respectively (δ_i is -5 to $-7‰$ at present), and ε_{TOC} is carbon isotope discrimination between carbonate and organic matter (long-term average is roughly 30‰). Carbon isotope values as high as $+28‰$, if representing the ocean composition, cannot be produced by high rates of organic matter burial alone since this would require the fraction of carbon buried as organic matter to be above 1. Shields et al. (2002) suggested that the following basinwide to global processes could have enhanced ^{13}C-enrichment beyond the effect of high rates of organic matter burial in Neoproterozoic carbonates deposited between the Sturtian and Marinoan glacial events: (a) an increase in δ_i due to the exposure and weathering of carbonate platforms during sealevel falls; (b) an increase in ε_{TOC} due to microbial reworking of primary organic matter (Hayes et al., 1999); (c) a ^{13}C-enrichment on the scale of a restricted basin; and (d) a steep depth gradient in $\delta^{13}C$ due to the redox stratification on the scale of the ocean or basin. We find no association between sealevel fall and carbon isotope excursions in the Paleoproterozoic. In fact, most Paleoproterozoic ^{13}C-enriched carbonates are in transgressive sequences. Basin configuration during the deposition of the L1 member is somewhat uncertain due to the small areal extent and poor outcrop of this member, but it belongs to the same basin as all other members for which we infer an open-marine setting. Little is known about the redox stratification or $\delta^{13}C$ gradient in the Paleoproterozoic oceans. However, it is most unlikely to be on the scale of ^{13}C-enrichment in the L1 member. On the other hand, microbial mineralization of primary organic matter and reincorporation of this ^{13}C-depleted carbon by methanotrophs and sulfide oxidizing bacteria would increase the ε_{TOC} (Hayes et al., 1999). This process is likely to be enhanced in an ocean with high burial rates of organic matter. Some ^{13}C-enriched carbonates reveal ε_{TOC} values as high as 37‰ (Karhu, 1993; Swart, 1999; Bekker et al., 2001a; Sreenivas et al., 2001). Even more ^{13}C-depleted organic matter could have been deposited in deeper water settings.

5. Slaughterhouse Formation, Sierra Madre

5.1. Description

The Slaugherhouse Formation is the uppermost unit of the Snowy Pass Group in the Sierra Madre and is in structural contact with underlying units in the type area north of the Rambler Guard station (Fig. 7). This group experienced amphibolite facies metamorphism (Divis, 1976), and the Slaughterhouse Formation is dismembered by thrusts and a complete section is not preserved. The lower part of the formation in the type section consists of yellow, red, buff, blue, and green massive dolomites that contain layers of quartzite and dark-green phyllite (Houston et al., 1992). Stromatolites are not present, and dolomites are fine-grained and massive with rare cross-bedding. Dolomites are overlain by black graphitic phyllites and the upper part of the section consists of fine-grained, chloritic calc-schist (Houston et al., 1992). The dolomitic member is about 400 m thick in the type section and the overlying phyllite and schist are about 100 m thick (Houston et al., 1992). Samples were collected from several outcrops in the type area (sec. 26, T. 14N, R. 86W; Fig. 7): 97-SL-1 to 5 at Location 2, 97-SL-6 and 7 at Location 3 and 97-SL-8 and 9 at Location 4.

5.2. Geochemical data and diagenesis

Eight dolomite samples and one organic-rich phyllite were analyzed in this survey (Table 1). The dolomites have highly variable Mn (228–1,842

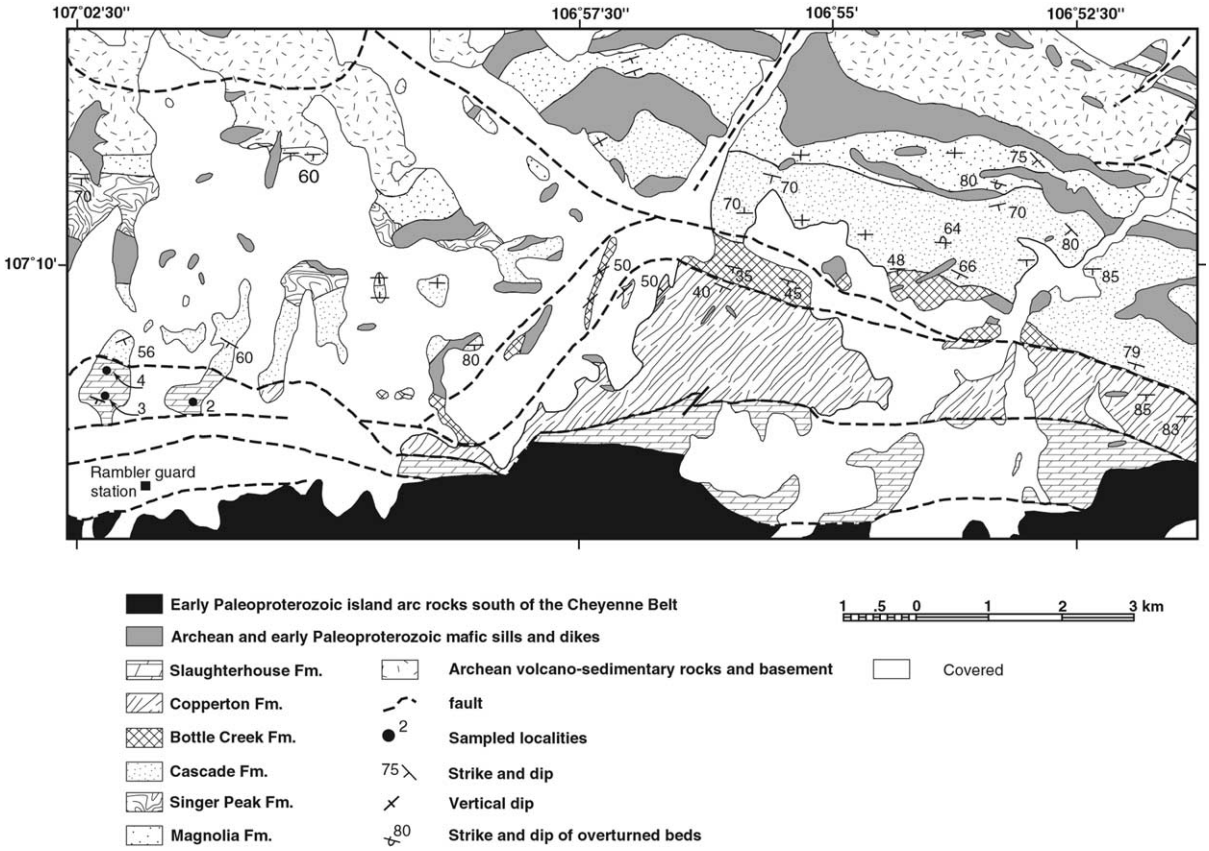

Fig. 7. Map of the type area of the Slaughterhouse Formation, Sierra Madre, showing sampled localities (map modified from Houston and Graff, 1995).

ppm) and low Sr contents (15–153 ppm). Oxygen isotope values display a narrow range between −10.3 and −14.6‰ (V-PDB) except for sample 97-SL-9 with a value of −4.2‰. Carbon isotope values range between +5.9 and +16.6‰. Two samples of cross-bedded pink/red dolomite from the lower part of the formation near to a fault contact (97-SL-8 and 9) have extreme carbon isotope compositions (+16.6 and +15.2‰, respectively) and the highest Mn contents and oxygen isotope values. An organic-rich phyllite (SL-97-5) collected above the dolomite member has high TOC content (19.3 mg C/g sample) and $\delta^{13}C_{org}$ value −22.6‰.

Given the higher metamorphic grade of the Slaughterhouse Formation samples, more negative $\delta^{18}O$ values are expected for the Slaughterhouse Formation samples, but they are very similar to those from the less metamorphosed Nash Fork Formation. This observation suggests that thick, and impermeable pure carbonates can, and in some cases, resist the oxygen isotope effects of regional metamorphism (cf. Valley and O'Neil, 1984; Bol et al., 1995). It is even more likely that there is good preservation of carbon isotope values. This observation suggests that dolomites may preserve a primary carbon isotope signal even at high metamorphic grade if dolomitization occurred early and carbonates were pure in composition. Carbon and oxygen isotope values of the Slaughterhouse dolomites are similar to those found in the L1 to M2 members of the Nash

Fork Formation. Two dolomite samples from the lower part of the Slaughterhouse Formation (97-SL-8 and 9) are comparable in carbon isotope values to those from the L1 member of the Nash Fork Formation. If the correlation of the Slaughterhouse Formation with the Nash Fork Formation is correct, it is likely that the recorded carbon isotope values reflect oceanic rather than local compositions.

6. Black Hills, South Dakota

6.1. Description

All Black Hills units experienced biotite grade metamorphism with the exception of carbonates from the Harney Peak Granite area which experienced sillimanite grade of metamorphism (inset in Fig. 3; Redden et al., 1990). The oldest unit of the Paleoproterozoic succession in the Black Hills—the Boxelder Creek Formation—outcrops near Nemo (Fig. 3) and belongs to the older rift sequence. Its contact with the underlying Nemo Iron Formation is not exposed, but is inferred to be unconformable based on the presence of BIF clasts in conglomerates of the Boxelder Creek Formation (Redden, 1980), whereas the contact with the overlying Benchmark Iron Formation is conformable. The lower part of the Boxelder Creek Formation consists largely of paraconglomerate, conglomerate, impure quartzite, shale, and minor dolomite. Overlying quartzites are up to 3.3 km thick and, locally, contain lenses of pyriferous, uraniferous conglomerates (Redden et al., 1990). Two ~30 m thick siliceous dolomite intervals in the lower part of the quartzite succession are separated by thin blue–gray phyllite (Redden, 1981). Samples from dolomite lenses and layers (SD-series) were collected at the Benchmark location (Location 1 in Fig. 3) and near the Nemo cemetery (Location 2 in Fig. 3). In addition, the lower and upper carbonate intervals were sampled further southeast along strike (B99-series; Location 3 in Fig. 3). B99 series samples were collected in stratigraphic order through the lower dolomite interval with a sampling interval of several meters.

A younger rift succession (Estes Formation) unconformably overlies the Benchmark Iron Formation and Boxelder Formation and consists of conglomerate overlain by quartzite (Redden, 1981). Siliceous fine- to medium-grained dolomite and phyllite occur in the middle part of the formation. Carbonate samples were collected at the intersection of Estes Creek Road and Estes Creek (SD-series; Location 4 in Fig. 3). Herringbone calcite structures (cf. Sumner and Grotzinger, 1996) were observed in one sample.

The Roberts Draw Formation, conformably overlying the Estes Formation, is 20–100 m thick and consists of dolomite gradationally overlain by limestone with interbedded dolomite and capped by graphitic, gray phyllite (Redden, 1981). Small (~5 cm height) domal stromatolites were rarely observed. Samples were collected on Forest Service Road 201 (SD-96-4; Location 5 in Fig. 3) and along the South Boxelder Creek (B99-series; Location 6 in Fig. 3). B99 samples were collected in stratigraphic order from the exposed lower part with a sampling interval of several meters. Rocks considered correlative with the Roberts Draw Formation outcrop near Bear Mountain in the Medicine Mountain area, and in large roof pendants of the Harney Peak Granite south of the Harney Peak (DeWitt et al., 1986, p. 13). Pure carbonates (HP-series; Location 7 in Fig. 3) were sampled from roof pendants of the Harney Peak Granite.

6.2. Geochemical data and diagenesis

Most studied samples are dolomites with the exception of several calcite samples from the Roberts Draw Formation. The degree of alteration as well as the geochemical signatures varies between units and the following descriptions are given separately for each.

Dolomites of the Boxelder Formation have high Mn contents (2,866–10,919 ppm) and variable but generally very low Sr contents (tr.–214 ppm). Fe content is high in two samples analyzed (10,297 and 27,430 ppm). $\delta^{18}O$ values range between −9.6 and −20.8‰; most samples are significantly depleted in ^{18}O suggesting significant exchange with hot metamorphic fluids. $\delta^{13}C$ values range

narrowly, however, between −1.8 and +1.1‰. Samples B99.1-6 collected from the lower dolomite interval have consistent $\delta^{13}C$ values between +0.5 and +1.1‰, whereas samples collected from the upper dolomite interval (B99.7 and 8) have negative $\delta^{13}C$ values between −1.4 and −0.1‰. The SD-series samples were likely stronger affected by metamorphism since their oxygen isotope values are significantly depleted relative to the B99 series samples. The consistency of the carbon isotope values in the high-resolution stratigraphic sampling suggests that primary $\delta^{13}C$ compositions have been retained, but with such degree of $\delta^{18}O$ depletion, caution should be taken in further interpretation of these values.

Dolomites of the Estes Formation have high Mn contents (515–12,118 ppm) and low Sr contents (tr.–149 ppm). One analyzed sample has a high Fe content (8,961 ppm). Oxygen isotope values are generally very low, as in the Boxelder Formation samples, with the exception of a single sample (Table 1). Carbon isotope values in the Estes Formation are enriched in ^{13}C relative to the underlying Boxelder Formation, by 1–2‰.

Calcites and dolomites of the Roberts Draw Formation have variable but generally intermediate Mn contents (394–2,720 ppm) and low Sr contents (tr.–106 ppm). One sample analyzed has a Fe content as high as 13,083 ppm. Oxygen isotope values range between −15.6 and −7.3‰, and are generally higher than those for carbonates of the Boxelder and Estes formations, suggesting lower degrees of metamorphism, and perhaps better preservation of $\delta^{13}C$ values. Except for one sample, carbon isotope values range between −0.4 and +1.9‰. Sample SD-96-4 has very low carbon and oxygen isotope values and high Fe and Mn content suggesting a higher degree of alteration than for other samples of the Roberts Draw Formation (Table 1).

Three dolomite samples from the roof complex of the Harney Peak Granite have relatively low Mn (103–282 ppm) and Sr (28–57 ppm) contents. Oxygen isotope values remarkably range between −5.4 and −8.1‰, and are higher than those in carbonates of the correlative Roberts Draw Formation. $\delta^{13}C$ values are between +2.1 and +2.3‰ and are also slightly higher than the highest $\delta^{13}C$ value (+1.9‰) in the Roberts Draw Formation.

The general depletion of ^{18}O in Black Hills carbonates is likely related to their impure composition, small thickness, and their position within thick siliciclastic successions, since the supracrustal sequence in the Nemo area experienced only biotite grade metamorphism (Redden et al., 1990). In contrast, higher oxygen isotope values in carbonates of the Roberts Draw Formation are likely related to the greater thickness and relatively pure composition of carbonates in this unit. Carbon isotope values of carbonates from the Black Hills area are on average close to 0‰, and broadly resemble values in carbonates from the upper Nash Fork Formation.

7. Whalen Group, Hartville Uplift

7.1. Description

The Whalen Group is formally subdivided into four formations in ascending order: (1) Mother Featherlegs Metabasalt; (2) Silver Springs Formation (subgraywacke and ferruginous, graphitic and pyritic schist containing layers and lenses of Lake Superior type BIF), (3) Wildcat Hills Formation (dolomite), and (4) Muskrat Canyon Metabasalt (Sims et al., 1997; Sims and Day, 1999). This stratigraphy was constructed on the basis of lithological correlation between the eastern and western domains of different metamorphic grade, structural complexity and, likely, depositional histories, resulting in one stratigraphic scheme for the two juxtaposed domains (Fig. 8). Our study suggests that carbonates from the Hartville Uplift do not belong to a single stratigraphic unit since they differ in their depositional environment, degree of metamorphism, and isotopic signatures (see Section 7.2). Structural complications and limited outcrop did not allow for the stratigraphic relationships between these distinctive carbonate units to be established in the field. The following discussion is focussed on three measured sections from the western domain augmented by observations in both domains.

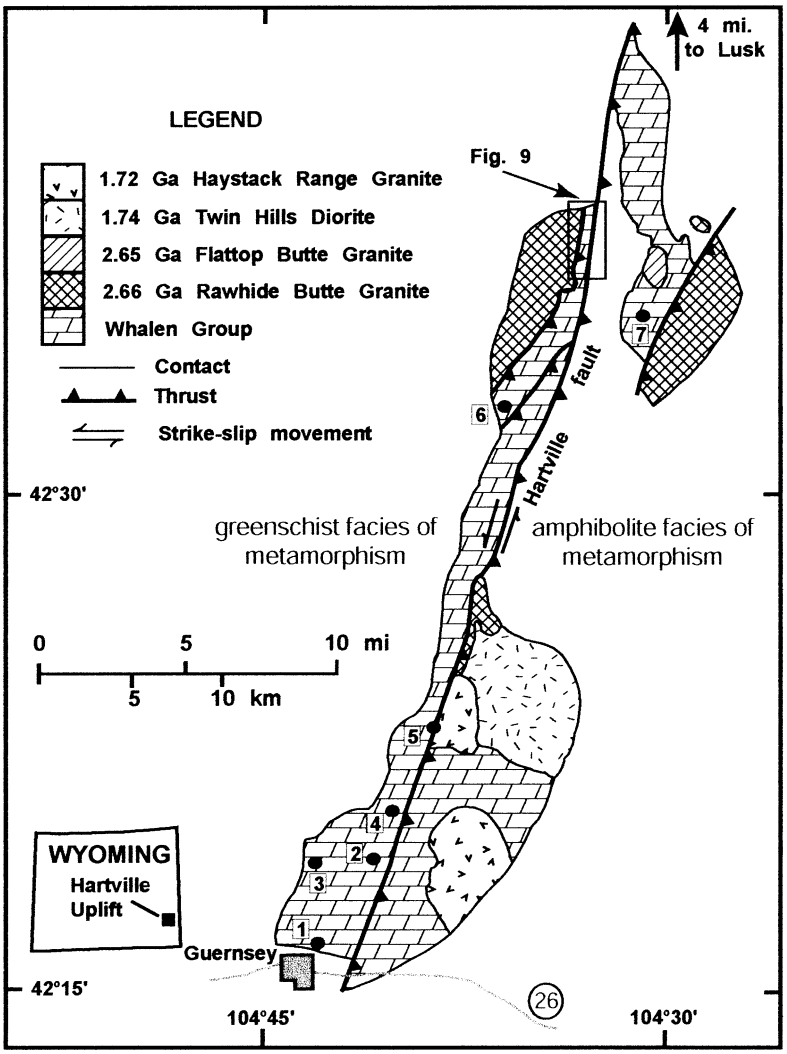

Fig. 8. Map of the Hartville Uplift, WY (modified from Sims and Day, 1999).

Several sections (Locations 8, 9 and 11 in Fig. 9) were measured and sampled in the western domain near the Rawhide Creek mouth where the Whalen Group is in structural contact with the Archean Rawhide granite. The most complete section in this area (Location 8 in Fig. 9) is cut by a fault with unknown, but likely minor, displacement. The lower part of this section extending up to the fault consists of an upward-deepening cycle of red ferruginous quartzites, argillites with thin layers of brown dolomite, and brown dolomite. Across the fault, gray massive dolomite with chert beds underlies an upward-shallowing cycle that includes from the base to the top: ribbon dolomite, pink–gray dolomite with silicified domal digitate stromatolites (forming a reef up to 30 m thick), pink dolomite, and dark calc-schist. The section immediately to the south of the Rawhide Creek mouth (Location 9 in Fig. 9) contains two levels with silicified domal digitate stromatolites making up smaller stromatolite reefs than in the first section. Hofmann and Snyder (1985) described *Hadrophycus* sp. stromatolites from these reefs. A third section, further south of the Rawhide Creek

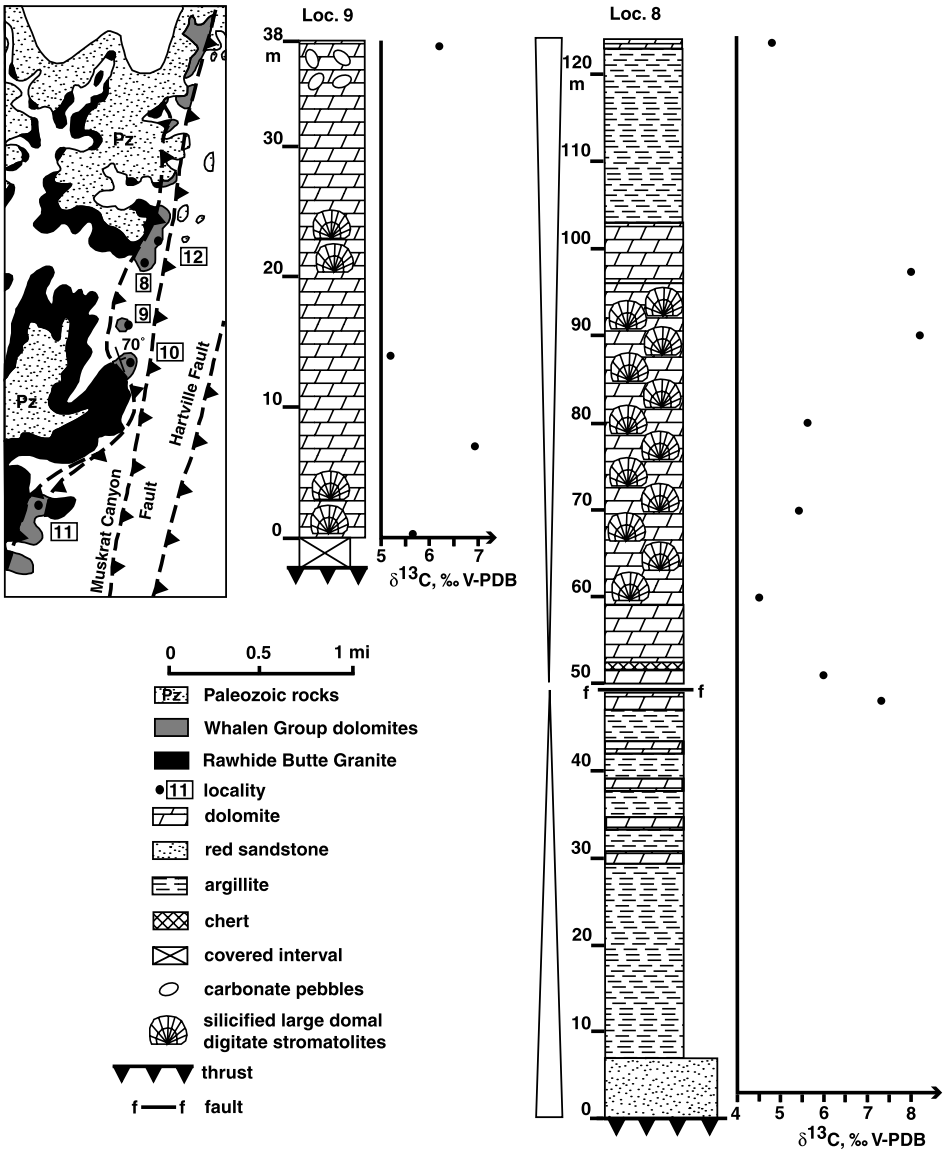

Fig. 9. Detailed map of the Rawhide Creek area, Hartville Uplift (from Sims and Day, 1999; Day et al., 1999), and measured sections and $\delta^{13}C$ values at localities 8 and 9.

mouth in a separate thrust sheet, consists of gray massive dolomite with three levels of large domal stromatolites without digitate structures (Location 11 in Fig. 9). Domal stromatolites have diameters up to 10 m and are only partially silicified.

Gray and pink massive dolomites were sampled on the northern limb of the Graves Ranch anticline and on its southern limb in the Sparks Canyon (Locations 2 and 3 in Fig. 8). Hofmann and Snyder (1985) observed stratiform and small-scale columnar stratiform stromatolites in this area. In addition, dolomites were sampled at several other locations in the western domain, including the Guernsey Quarry (Location 1 in Fig. 8) where they experienced higher metamorphic grade and contain tremolite 'turkey tail' structures

Table 3
Correlation between studied Paleoproterozoic successions, Huronian and Marquette Range supergroups (after Houston et al., 1992 with additional chemostratigraphic constraints from this study)

Event stratigraphy	Huronian Supergroup, Ont., Canada	Marquette Range Supergroup, MI	Snowy Pass Supergroup, WY	Snowy Pass Group, Sierra Madre, WY	Nemo Succession, Black Hills, SD	Whalen Group, Hartville Uplift
Fine-grained siliciclastic units			French Slate		Gingrass Draw Slate and Buck Mountain Quartzite	
Mafic volcanism with ages ~2.0–1.95 Ga			Towner Greenstone		Unnamed mafic volcanic unit	Muskrat Canyon Metabasalt
Carbonates with $\delta^{13}C$ values close to 0‰			Upper part of the Nash Fork Formation		Estes and Roberts Draw formations	Wildcat Hills Formation
Black organic-rich shales with BIFs			M1 and M3 members of the Nash Fork Formation	Upper part of the Slaughterhouse Formation		Silver Springs Formation
Carbonates with $\delta^{13}C$ values between +6 and +10‰			Lower part of the Nash Fork Formation except the L1 member	Slaughterhouse Formation except the lower part		Carbonates in the Rawhide Creek area
Carbonates with $\delta^{13}C$ values above +10‰			L1 member of the Nash Fork Formation	Lower part of the Slaughterhouse Formation		
Carbonates with $\delta^{13}C$ values between +4 and +8‰	Gordon Lake Formation					
Mature Al-rich hematite-bearing quartzites and carbonates with $\delta^{13}C$ values < +4‰	Lorrain Formation	Randville Dolomite Sturgeon Quartzite	Medicine Peak Quartzite	Copperton Formation		
Third glacial horizon	Gowganda Formation	Fern Creek Formation	Headquarters Formation	Bottle Creek Formation		
Second glacial horizon overlain by carbonate unit	Espanola Formation		Vagner Formation	Bottle Creek Formation		
Second glacial horizon	Bruce Formation		Vagner Formation	Bottle Creek Formation		
First glacial horizon	Ramsay Lake Formation		Campbell Lake Formation	Singer Peak Formation		
Pyrite and uraninite-rich mature quartzites	Matinenda Formation		Lindsey Quartzite and Magnolia Formation	Magnolia Formation	Boxelder Formation	

and chert layers and nodules, but lack stromatolites. The base of the carbonate succession in this area overlies amphibolite. In the eastern domain, recrystallized dolomites were sampled in the Copperbelt-Omaha mine area (Location 7 in Fig. 8). Poorly preserved stratiform stromatolites up to 1 m in size rarely occur in this area.

7.2. Geochemical data and diagenesis

All analyzed samples are dolomites (Table 1) with low Sr contents (tr.–136 ppm) and highly variable Mn contents (35–3,286 ppm). Fe contents measured in four samples are also high (988–6,381 ppm). Oxygen isotope values range between −4.2 and −15.0‰, and show, on average, greater ^{18}O enrichment than dolomites of the Nash Fork Formation. Carbon isotope values of carbonates are bimodal. Carbonates from the Rawhide Creek area show ^{13}C-enrichment up to +8.2‰ whereas carbonates from all other localities have $\delta^{13}C$ values between −0.3 and +3.2‰. Notably, the $\delta^{13}C$ compositions of Hartville samples are negatively correlated with their $\delta^{18}O$ compositions, opposite to the expected diagenetic trend. Samples with the lowest oxygen isotope values are also most enriched in manganese. The levels of ^{13}C-enrichment and ^{18}O-depletion in carbonates of the Rawhide Creek area are similar to those in the lower Nash Fork Formation, and we interpret these units as broadly time equivalent.

8. Implications for global correlation

The Deep Lake and lower Libby Creek groups are considered correlative with the Huronian Supergroup in Ontario, Canada, based on the presence in both successions of (1) ca. 2.48–2.45 Ga old conglomerates with detrital pyrite and

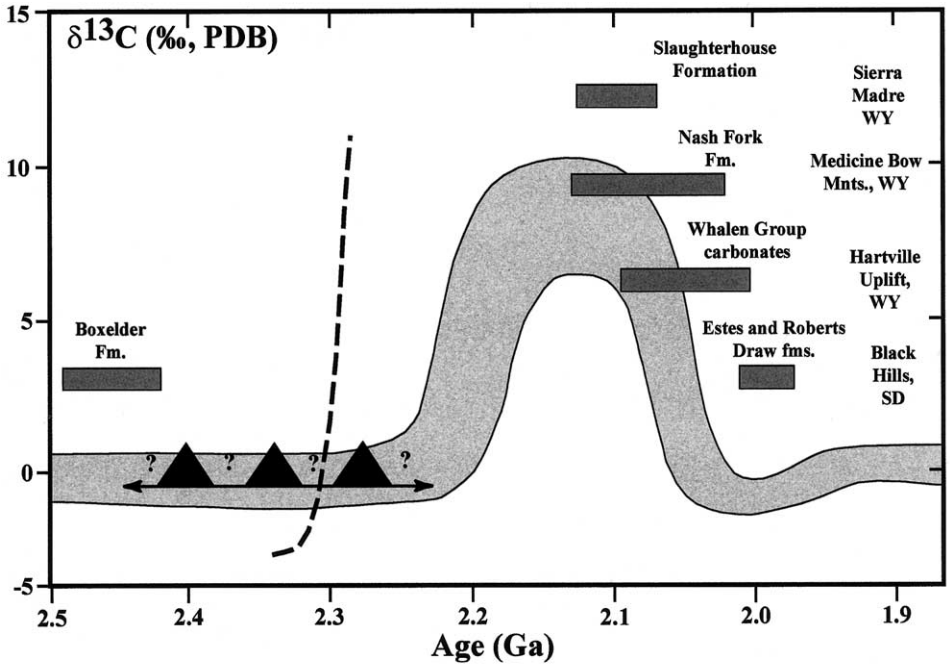

Fig. 10. Schematic representation of Paleoproterozoic secular carbon isotope variations after Karhu and Holland (1996) with additional information from Bekker et al. (2001a) shown by dashed line. Black triangles and question marks between them represent three Paleoproterozoic glacial events in North America and their age uncertainties. Studied units are arranged along the horizontal axis according to their geochronologic, lithostratigraphic, and chemostratigraphic age constraints (see text for discussion).

uraninite followed by three glacial horizons; (2) a carbonate unit above the middle of three diamictites, and (3) thick, mature, Al-rich hematite-bearing quartzites above the uppermost glacial horizon (Houston et al., 1992; Roscoe and Card, 1993; Table 3).

Correlation between the upper Libby Creek Group in the Medicine Bow Mountains and other Paleoproterozoic sedimentary successions is more ambiguous. Based on the chemostratigraphic data presented above and available event stratigraphy, we speculate, with caution, correlations with other successions worldwide. To do so, however, requires knowledge of Paleoproterozoic trends in carbon isotope variations, which are currently in a state of flux given a proliferation of chemostratigraphic and geochronologic studies. Karhu and Holland (1996) recognized that post-glacial carbonates with ages between 2.2 and 2.1 Ga have carbon isotope values as high as +10‰. These authors compiled a curve of secular carbon isotope variations with a single long-lasting peak between 2.2 and 2.1 Ga. This view was modified with the recent discovery of marine carbonates with carbon isotope values up to +10.4‰ in the upper part of the Duitschland Formation, sandwiched between two Paleoproterozoic glacial diamictites in South Africa (Buick et al., 1998; Bekker et al., 2001a). The Duitschland peak although found to date in only one basin, likely represents a global event (Bekker et al., 2001a). Carbon isotope values as high as +3.5‰ have been recognized in truncated carbonates beneath the basal Duitschland Formation diamictite (Tongwane Formation; Bekker et al., 2001a), but similar or greater ^{13}C-enrichments have not yet been found in any pre-glacial strata worldwide. A two-peak curve of secular carbon isotope variations with one long-lasting peak between 2.2 and 2.1 Ga and another possible peak of undetermined duration during the Paleoproterozoic glacial epoch (Fig. 10) was modified by Melezhik et al. (1999a) who presented a curve with three to four peaks based on data from South African successions (Buick et al., 1998) and the Pechenga Basin, Kola Peninsula, Russia. As discussed by Bekker et al. (2001a), the South African data contain evidence for only two carbon isotope excursions based on revised stratigraphic and age constraints. Melezhik et al. (1999a) placed the Kolasjoki Sedimentary Formation of the Pechenga Basin in the midst of the 2.2–2.1 Ga extended event (Karhu and Holland, 1996). This formation contains carbonates with δ^{13}C values ranging between −7.8 and +2.0‰ (Melezhik and Fallick, 1996), but has very poor age constraints (2114±52 Ma Rb/Sr whole rock age on the overlying mafic volcanics; Balashov, 1996). We believe that this unit cannot be used as evidence for more than one excursion during the 2.2–2.1 Ga event, and was more likely deposited in the aftermath of this excursion based on lithologic (Mn-rich carbonates and phosphorites) and chemostratigraphic considerations. The tentative correlations presented here are based on the two-peak curve, but we recognize that further study might modify this evolving trend.

The Nash Fork Formation is younger than the Paleoproterozoic glacial epoch and the succeeding climatic amelioration indicated by the presence of thick, mature, Al-rich quartzites. The extreme δ^{13}C values at the base of this unit (L1 member) likely correspond to highly ^{13}C-enriched carbonates in Karelia, Russia (up to +18‰; Melezhik et al., 1999a) and in other Paleoproterozoic carbonate successions worldwide (Table 2). These carbonate successions have poor age constraints with the exception of the Seward and Pistolet subgroups of the Kaniapiskau Supergroup, New Quebec Orogen, which are well constrained between 2169±2 and $2142^{+4}/_{-2}$ Ma (Rohon et al., 1993; Melezhik et al., 1997b). Carbonate units with carbon isotope values of the same magnitude as those found in the L2 through M2 members of the Nash Fork Formation (between +6 and +8‰) also occur in Fennoscandia where they are better constrained in age to ca. 2.2–2.1 Ga (Karhu, 1993). Globally, Paleoproterozoic carbonate units correlative with the Nash Fork Formation based on similar carbon isotope systematics are also known, as discussed above from South Africa (Master et al., 1993; Buick et al., 1998; Swart, 1999; Bekker et al., 2001a) as well as Gabon (Gauthier-Lafaye and Weber, 1989), Zimbabwe (Bekker et al., 2001b), Australia (Lindsay and Brasier, 2002), India (Sreenivas et al., 2001), Scotland (Baker and Fallick, 1989a), Brazil (Sial et al.,

2000), Russia (Akhmedov et al., 1996), and North America (Melezhik et al., 1997a; Bekker, 1998; Hofmann and Davidson, 1998).

The change in carbon isotope values at the level of the M3 member from high values to those near 0‰ was accompanied by deposition of black organic-rich shale (upper carbonaceous shale member with TOC content up to 203.6 mg C/g sample). Similar changes in carbon isotope values of carbonates accompanied by deposition of black organic-rich shales are described in Fennoscandia (Karhu, 1993; Melezhik et al., 1999b), Gabon (Francevillian Series; Weber et al., 1983; Gauthier-Lafaye and Weber, 1989), and Quebec (Lower Albanel Formation; Mirota and Veizer, 1994; Bekker et al., 1997). The end of the carbon isotope excursion in Fennoscandia is constrained between 2062±2 and 2113±4 Ma (Karhu, 1993). Age constraints for the Francevillian Series, Gabon (Bros et al., 1992), agree with the Fennoscandian age constraints for the end of the biogeochemical anomaly. In addition, the end of the carbon isotope excursion in the upper part of the Pretoria Group, South Africa, preceded intrusion of the Bushveld complex and the associated Rooiberg Felsites dated at 2061±2 Ma (Walraven, 1997; Bekker et al., 2001a). A minimum age for the Nash Fork Formation is constrained by the younger mafic volcanism that has been dated elsewhere on the Wyoming Craton to approximately 2.0–1.97 Ga (Redden et al., 1990; Cox et al., 2000). Combined, these age constraints suggest that the Nash Fork Formation was deposited between ca. 2.2 and 1.97 Ga.

Based on lithostratigraphic considerations, Houston et al. (1992) suggested that the Nash Fork Formation in the Medicine Bow Mountains and the Slaughterhouse Formation in the Sierra Madre are correlative. Chemostratigraphic data presented above support the equivalence of the Slaughterhouse Formation and the lower Nash Fork Formation since both units contain carbonates with high $\delta^{13}C$ values, including values above +10‰ (Table 3). However, a limited number of samples and poor outcrop of the Slaughterhouse Formation precludes speculation that time equivalents of the upper Nash Fork Formation are absent in the Sierra Madre.

Houston et al. (1992) also correlated the Nash Fork Formation with the Gordon Lake and Bar River formations of the Huronian Supergroup and the Randville Dolomite of the Marquette Range Supergroup, Michigan. This correlation is not supported by chemostratigraphic data since the change in carbon isotope trend in the middle Nash Fork Formation suggests that its deposition straddled the end of the ca. >2.2–2.1 carbon isotope excursion whereas the Huronian Supergroup is intruded by the 2219.4±3.5 Ma old Nippissing sills (U–Pb zircon; Corfu and Andrews, 1986) and both formations were likely deposited at the beginning of the extreme carbon isotope anomaly. Correlation with the Randville Dolomite, Marquette Range Supergroup is also unlikely because the Randville Dolomite is considered correlative with the Gordon Lake Formation of the Huronian Supergroup, ON, based on its conformable stratigraphic position above the glacial diamictite and mature quartzite unit (Young, 1983).

The Boxelder Formation and Benchmark Iron Formation were likely deposited before the glacial epoch but after the initial rifting of Kenorland at ca. 2.48–2.45 Ga, based on their unconformable position above Archean rocks, the presence of uranium- and pyrite-rich conglomerates in the Boxelder Formation, and a major unconformity above the Benchmark Iron Formation, and a lack of evidence for glacial influence on sedimentation. Carbonates of the Boxelder Formation and BIFs of the Benchmark Iron Formation are unique to the Wyoming Craton since North American Paleoproterozoic successions with similar age do not contain these lithologies. Lithostratigraphic and chemostratigraphic data as well as age constraints suggest correlation between the Estes and Roberts Draw formations in the Black Hills, SD, and the upper Nash Fork Formation (Table 3). Both successions are overlain by mafic volcanic rocks, slates, and quartzites. The Ellison Formation in the Lead area that is considered correlative with the Buck Mountain Formation and Gingrass Draw Slate of the Nemo area (DeWitt et al., 1986) contains at the base felsic metatuff dated at 1974±8 Ma (U–Pb zircon; Redden et al., 1990). In addition, carbonates in the Roberts Draw,

Estes, and upper Nash Fork formations have $\delta^{13}C$ values between 0 and +3‰ (Table 1). However, the possibility that the Roberts Draw and Estes formations are younger than the Nash Fork Formation cannot be dismissed. Carbonates of the Whalen Group in the Rawhide Creek area are likely correlative with the lower Nash Fork Formation based on similar chemostratigraphic characteristics ($\delta^{13}C$ values up to +8‰) as well as similar stromatolite morphologies. Carbon isotope values up to +8‰ are unknown from well-dated Archean carbonates but typical for Paleoproterozoic carbonates with an age between 2.22 and 2.1 Ga (Karhu and Holland, 1996). Other lithologies of the Whalen Group including carbonates with $\delta^{13}C$ values close to 0‰, mafic volcanic rocks and ferruginous slates might be correlative with carbonates of the upper Nash Fork Formation, Towner Greenstone, and French Slate, respectively. However, the possibility that some parts of the Whalen Group may be Archean in age cannot be excluded based on available data. Higher metamorphic grade supracrustal rocks in the eastern domain intruded by the Archean Flattop Butte Granite, supracrustal enclaves in the Archean Rawhide Butte Granite, and the higher metamorphic grade succession near Guernsey (Location 1 in Fig. 8) could well be Archean in age.

9. Tectonic implications

This study has three implications for understanding the Paleoproterozoic tectonic history of the Wyoming Craton: (1) the Paleoproterozoic passive margin on the southern flank of the Wyoming Craton extended from the Sierra Madre through the Medicine Bow Mountains to the Hartville Uplift; (2) rifting and breakup on the eastern flank of the Wyoming Craton and opening of the Manikewan ocean (sensu Stauffer, 1984) coincided with or closely followed the end of the Paleoproterozoic carbon isotope excursion between 2.11 and 2.06 Ga; (3) rifting and breakup on the eastern flank of the Wyoming Craton dissected and reactivated the mature passive margin on the southern flank of the Wyoming Craton.

Karlstrom et al. (1983) suggested that the upper Libby Creek Group in the Medicine Bow Mountains was deposited in a foreland basin based on upward-deepening trend and mafic volcanism (Towner Greenstone) at the top of the succession. This interpretation was not confirmed by recent Sm–Nd and REE provenance studies that have shown an Archean source for the upper Libby Creek Group, and no evidence for proximity to the Paleoproterozoic volcanic arc (Ball and Farmer, 1991; Crichton and Condie, 1993). This study constrains the age of the Nash Fork Formation between 2.2 and 1.97 Ga. Consequently, the upper Libby Creek Group is significantly older than the 1.74–1.78 Ga volcanic arc (Chamberlain, 1998) that collided with the southern flank of the Wyoming Craton and was likely deposited on a passive margin. Lithostratigraphic and chemostratigraphic data suggest correlation between passive margin carbonate deposits of the Sierra Madre, Medicine Bow Mountains, and Hartville Uplift. Two carbonaceous shale members in the middle part of the Nash Fork Formation represent drowning events associated with the reactivation of the old, mature passive margin on the southern flank of the Wyoming Craton by rifting and breakup along the eastern flank of the Wyoming Craton (Bekker and Eriksson, in press).

The age of rifting and breakup on the eastern flank of the Wyoming Craton is poorly constrained. Mafic intrusives and their felsic differentiates on the southern flank of the Wyoming Craton likely related to this event are between 2.0 and 2.1 Ga in age (Premo and Van Schmus, 1989; Cox et al., 2000). The only exposed area on the eastern flank of the Wyoming Craton is in the Black Hills, SD. Initiation of the younger rift basin there was likely related to the 2.1–2.0 Ga rifting and final breakup of the Kenorland supercontinent (Aspler and Chiarenzelli, 1998). The younger rift succession unconformably overlies the older rift succession intruded by and infolded with the 2170 ± 120 Ma old Blue Draw Metagabbro (U–Pb zircon; Redden et al., 1990). Recognizable 2025 ± 50 Ma old overgrowths on Archean zircons were likely formed in response to younger rifting event (U–Pb zircon; McCombs et al., 2001). The base of the younger rift succession (Estes Formation) is

Table 4
Environmental indicators within Paleoproterozoic successions with ca. 2.1 Ga ages based on geochronologic and chemostratigraphic constraints

Name of the succession and location	BIF	Mn-rich lithologies	Organic-rich shales	Most depleted $\delta^{13}C_{org}$ values	Phosphorites	Mafic volcanics	Reference to age and $\delta^{13}C_{carb}$ values $> +4‰$
Nash Fork Formation, WY, USA	Thin discontinuous BIF (Bekker and Eriksson, in press)		Black organic-rich shales (Bekker and Eriksson, in press)			Overlain by Towner Greenstone	This study
Lower Albanel Formation, Mistassini Basin, Quebec, Canada			Mirota and Veizer (1994)	−39.0‰ (Bekker et al., unpubl.)			Mirota and Veizer (1994), and Bekker et al., unpubl.
Ludikovian Group, Fennoscandian Shield	Laajoki and Saikkonen (1977), Paakola (1971)	Paakola (1971), Golubev et al. (1984)	Shungites (Karhu, 1993; Melezhik et al., 1999b)	−44.4‰ (Karhu, 1993; Melezhik et al., 1999b)	Äikäs (1980), Gehör (1994), Bekasova and Dudkin (1982), Golubev et al. (1984), Melezhik and Predovsky (1982)	Karhu (1993), Melezhik et al. (1999b), Hanski et al. (2001)	Karhu (1993), Melezhik and Fallick (1996)
Hapschan Group, Anabar Shield, Russia		Rhodonite and spessartine (Ponomarenko, 1973)	Ponomarenko (1973)		Apatite (Ponomarenko, 1973)	Ponomarenko (1973), Rozen et al. (1990)	Rozen et al. (1990, 1994)
Fyedorov Suite, Aldan Supergroup, Aldan Shield, Russia	Salop (1982), Pavlov et al. (1987)	Mn-rich silicates (Kulish, 1970)	Kulish (1970)		Apatite (Salop, 1982; Guliy, 1995a Guliy, 1995b)	Rundqvist and Mitrofanov (1993)	Sidorenko and Borshchevsky (1977); Guliy (1995a,b)
Slyudyanka crystalline complex, Eastern Siberia, Russia		Rhodonite, bustamite and spessartine (Reznitsky et al., 1976; Koneva et al., 1998)	Yudin and Arsenev (1970)		Apatite (Yudin and Arsenev, 1970)	Yudin and Arsenev (1970), Kotov et al. (2000)	Borshchevsky et al. (1982), Reznitsky et al. (1998), Kotov et al. (2000)
Upper Yakovlevskaya and Timskaya suites, Oskolskaya Series (= Vorontzovskaya Series), KMA, Russia	Hematite- and martite-rich slates (Nikitina and Shchipanskiy, 1987)	Mn-rich sulfides in carbonates and slates (Lazur et al., 1981)	Sozinov and Kazantsev (1978), Zhmur and Stepanova (1987)	−44.2‰ (Sozinov et al., 1988; Lobzova and Esikov, 1981)	Phosphatic slates and quartzites (Sozinov and Kazantsev, 1978; Nikitina and Shchipanskiy, 1987)	Sozinov and Kazantsev (1978)	Schipansky and Bogdanova (1996), Akhmedov et al. (1996)
Temryukskaya Suite, Central Periazov Series, Central Periazov Syncline, Ukraine	Boiko et al. (1989)	Rhodonite (Kanygin et al., 1969; Kravchenko, 1993)	Kanygin et al. (1969), Boiko et al. (1989)	−35.3‰ (Sidorenko et al., 1972)	Apatite (Kanygin et al., 1969)		Boiko et al. (1989), Zagnitko and Lugovaya (1985, 1989), Schipansky and Bogdanova (1996)

Table 4 (*Continued*)

Name of the succession and location	BIF	Mn-rich lithologies	Organic-rich shales	Most depleted $\delta^{13}C_{org}$ values	Phosphorites	Mafic volcanics	Reference to age and $\delta^{13}C_{carb}$ values $> +4‰$
Gdantzevskaya Suite, Krivorozhskaya Series, Krivoy Rog, Ukraine	Boiko et al. (1989)		Prilutzky et al. (1992)	−36.3‰ (Yatsenko et al., 1986)			Boiko et al. (1989), Zagnitko and Lugovaya (1985), Prilutzky et al. (1992)
Hoshchevat-Zavalsk Suite, Bugskaya Series, Ukraine	Boiko et al. (1989)	Rhodochrosite (Shnyukov and Orlovsky, 1980; Varentsov and Rakhmanov, 1980; Kulish et al., 1988)	Zagnitko and Lugovaya (1986), Boiko et al. (1989)	−35.8‰ (Zagnitko and Lugovaya, 1986)	Apatite (Zagnitko and Lugovaya, 1989)	Boiko et al. (1989), Zagnitko and Lugovaya (1985)	Boiko et al. (1989), Zagnitko and Lugovaya (1985, 1989)
	Boiko et al. (1989), Zagnitko and Lugovaya (1985, 1989)						
Rodionovskaya Suite, Ingulo-Inguletzkaya Series, Ukraine		Kulish et al. (1988)	Graphitic schists (Boiko et al., 1989)		Apatite in quartzites (Yur'ev, 1968)	Overlies mafic volcanics (Kulish et al., 1988)	Zagnitko and Lugovaya (1985, 1989), Boiko et al. (1989)
Francevillian Series, Gabon	Leclerc and Weber (1980)	Rhodochrosite (Leclerc and Weber, 1980; Hein et al., 1989; Hein and Bolton, 1993)	Gauthier-Lafaye and Weber (1989)	−46.2‰ (Weber et al., 1983)	High phosphate content of iron formation (Leclerc and Weber, 1980)	Weber (1972)	Gauthier-Lafaye and Weber (1989), Bros et al. (1992)
Birimian Supergroup, West Africa (Nsuta, Ghana; Tambao, Birkina Faso; Mokta and Ziemougoula, Côte d'Ivoire)		Rhodochrosite (Dzigbodi-Adjimah and Sogbor, 1993; Weber, 1997; Mücke et al., 1999)	Mücke et al. (1999)			Mücke et al. (1999)	Master et al. (1993), Davis et al. (1994), Hirdes and Davis (1998)
Lukoshi Complex, Zaire		Mn-rich carbonates (Doyen, 1973, 1974)	Doyen (1973, 1974)			Doyen (1973, 1974)	André (1993), Feybesse et al. (1998)
Upper Lomagundi/Piriwiri Group, Zimbabwe	Oxide- and silicate-facies iron formations (Master, 1991)	Mn-oxides (Master, 1991)	Black graphitic slates (Master, 1991)		Phosphate-bearing shale (Master, 1991)	Overlain by andesitic volcanics (Master, 1991)	Schidlowski et al. (1976), Master (1991), Schidlowski and Todt (1998), Bekker et al. (2001b)

Table 4 (*Continued*)

Name of the succession and location	BIF	Mn-rich lithologies	Organic-rich shales	Most depleted $\delta^{13}C_{org}$ values	Phosphorites	Mafic volcanics	Reference to age and $\delta^{13}C_{carb}$ values > +4‰
Horseshoe basin, Nabberu Province, western Australia	Iron-rich shale (Krapez and Martin, 1999)	Mn-oxides and carbonates (Krapez and Martin, 1999)	Krapez and Martin (1999)			Krapez and Martin (1999)	Russell (1992), Woodhead and Hergt (1997), Krapez and Martin (1999) and Bekker et al., unpubl.
Aravalli Group, India	Nayak (1980)	Mn-oxides (Nayak, 1980; Roy, 1980)	Carbonaceous phyllites (Banerjee, 1971)		Stromatolitic phosphorites (Banerjee, 1971)		Maheshwari et al. (1999), Sreenivas et al. (2001), Banerjee et al. (1986)

older than a metagabbro sill dated at 1974±8 Ma (U–Pb zircon; Redden et al., 1990), which intrudes the overlying Roberts Draw Formation. Carbonates from the middle part of the Estes Formation have $\delta^{13}C$ values similar to those in the upper Nash Fork Formation suggesting that rifting on the eastern flank of the Wyoming Craton occurred either very late during the carbon isotope excursion or shortly thereafter.

10. Implications for the end of the carbon isotope excursion

This study supports earlier suggestions based on Fennoscandian data that the end of the carbon isotope excursion closely accompanied breakup of the Kenorland supercontinent at ca. 2.1 Ga (Karhu, 1993). Also, in common with the Fennoscandian record (Karhu, 1993; Melezhik et al., 1999b), deposition of organic-rich shales and thin, discontinuous BIF in the M3 member of the Nash Fork Formation straddled the end of the biogeochemical event. On a global scale, successions straddling the end of the $\delta^{13}C$ positive anomaly contain organic-rich shales, BIFs, Mn-rich lithologies, and phosphorites (Table 4). $\delta^{13}C$ values of organic carbon in the Francevillian and Fennoscandian carbonaceous shales deposited after the end of the carbon isotope excursion show a consistent decrease upsection to about −45‰ (Weber et al., 1983; Karhu, 1993; Melezhik et al., 1999b). The end of the carbon isotope excursion was also accompanied by voluminous mafic volcanism (Table 4). Melezhik et al. (1997a) argued for a decline in stromatolite abundance and diversity on the Fennoscandian Shield at the same time and a similar decline was inferred from Indian and Chinese data (Semikhatov and Raaben, 1994). A short-term decline in stromatolite abundance after the carbon isotope excursion was also observed in the U1 member of the Nash Fork Formation (Bekker and Eriksson, in press) and in the Lower Albanel Formation, Quebec, Canada. Although the significance of this change in stromatolite abundance and diversity is disputable (see Semikhatov and Raaben, 1996; Semikhatov et al., 1999; Awramik and Sprinkle, 1999), conditions for

stromatolite growth after the carbon isotope excursion were clearly unfavorable on several continents for at least a short period of time.

The presence of these lithologies and paleoenvironmental indicators in a consistent stratigraphic position with respect to the biogeochemical anomaly in several successions worldwide argues for a major oceanographic reorganization. Mn-rich lithologies, phosphorites, and BIFs common in late Neoproterozoic to early Cambrian successions have been attributed to the ocean overturn either at the end of glaciations (Kaufman et al., 1991; Klein and Beukes, 1993; Bühn and Stanistreet, 1997) or at the Precambrian/Cambrian boundary following the supercontinent breakup (Donnelly et al., 1990; Cook, 1992; Hein et al., 1999). Ocean overturns invigorated circulation in the otherwise anoxic Neoproterozoic ocean in which burial rates of organic carbon were high as inferred from highly positive carbon isotope values in carbonates (Knoll et al., 1986; Kaufman and Knoll, 1995; Hoffman et al., 1998). Controls on ocean anoxia remain conjectural. On the one hand, high hydrothermal and volcanic inputs of reduced elements to seawater (as recorded in mantle-dominated $^{87}Sr/^{86}Sr$ values in seawater proxies; cf. Asmerom et al., 1991) and the atmosphere would scrub out photosynthetically produced oxygen, but the balance of these two fluxes is unconstrained. Alternatively, Knoll et al. (1996) argue that widespread anoxia in the ocean may also be caused by a decrease in the rate of ocean circulation as a result of the low latitude position of landmasses coupled with a greenhouse climate.

Highly positive carbon isotope values (Tables 3 and 4; Karhu and Holland, 1996) in ca. 2.2–2.1 Ga open marine carbonates suggest high relative burial rates of organic matter in ocean sediments, which was likely aided by deep water anoxia and the development of extensive continental margins following rifting (cf. Des Marais, 1994; Hoffman et al., 1998). The lower carbonaceous shale member of the Nash Fork Formation (M1) sandwiched within the ^{13}C-enriched carbonates provides the first direct evidence that deposition of shallow water, ^{13}C-enriched carbonates was accompanied by high burial rates of organic carbon in deeper waters. Deposition of phosphorites, Mn-rich lithologies, and BIFs at the end of the carbon isotope excursion suggests limited mixing between the deep and shallow parts of the ocean during the Paleoproterozoic carbon isotope excursion (cf. Klein and Beukes, 1993). Whereas Mn and Fe were supplied to the deep ocean through hydrothermal activity at MORs, phosphorus was likely released from organic matter and ferric oxyhydroxides in anoxic settings (Van Cappellen and Ingall, 1994; Ingall and Jahnke, 1994). BIFs deposited at the end of the ca. 2.2–2.1 Ga carbon isotope excursion are thin, lean, and incomparable in size to those preserved in older (ca. 2.45 Ga old) or younger (1.9–1.8 Ga old) successions (Isley, 1995; Simonson and Hassler, 1996; Isley and Abbott, 1999; Table 4). This observation implies that Fe flux into the deep ocean exceeded the H_2S content in the ocean during the carbon isotope excursion (Canfield, 1998), which might be related to either low sulfate content in the ocean (Canfield and Raiswell, 1999) or low rates of sulfate delivery to the deep ocean due to sluggish circulation. In contrast to BIFs, manganese deposits postdating the carbon isotope excursion are large. A likely explanation is that the iron content was controlled by sulfate reduction and subsequent precipitation of pyrite in the deep ocean, thereby separating Fe and Mn in seawater. Sulfate reduction also led to high deep ocean carbonate-alkalinity enriched in ^{12}C (Canfield and Raiswell, 1991; Knoll et al., 1996; Grotzinger and Knoll, 1995).

The temporal relationship between the end of the carbon isotope excursion and Kenorland breakup suggests that ocean circulation was invigorated by changes in land distribution related to opening of new seaways and continent movement to high latitudes. Driven by this factor, deep ocean waters charged with carbonate alkalinity and nutrients (P, Fe, and Mn) may have encroached onto shelves. Mixing with deep ocean waters enriched in ^{12}C shifted the carbon isotope composition of shallow waters to near 0‰ as shown by carbonates from the upper Nash Fork Formation (Fig. 5). Carbon isotope values as low as −20‰ in carbonates associated with organic-rich shales straddling the end of the carbon isotope excursion on the Fennoscandian Shield and Voronezh Massif, Russia, are likely related in part to

diagenetic and metamorphic processes (Zhmur and Stepanova, 1987; Sozinov et al., 1988; Yudovich et al., 1990; Karhu, 1993; Melezhik et al., 1999b), but might also record upwelling of deep waters highly depleted in ^{13}C. A high nutrient flux to shallow waters likely enhanced productivity locally. This increase in productivity might explain the apparent stromatolite decline since abundant planktonic forms in shallow waters would decrease water transparency confining stromatolites to very shallow areas within basins (cf. Hallock and Schlager, 1986). The chemostratigraphic record of the upper Nash Fork Formation suggests that the carbon isotope composition of the ocean was relatively stable near 0‰ after the end of the carbon isotope excursion despite ocean overturn and the effects of localized areas with high productivity. Iron and manganese were deposited as oxides and carbonates once they entered oxygenated and alkaline shallow waters (Hein et al., 1989; Yeh et al., 1995a,b; Hein and Bolton, 1993).

The upward trend towards more negative carbon isotope values in organic carbon from carbonaceous shales overlying ^{13}C-rich carbonates in the Francevillian and Fennoscandian basins (Weber et al., 1983; Karhu, 1993; Melezhik et al., 1999b) could be explained by release of methane clathrates during the ocean overturn (cf. Dickens et al., 1997; Dickens, 2001; Kennedy et al., 2001). However, this trend persists over large thicknesses ($\sim$ 800 m in Karelia, Russia; Melezhik et al., 1999b) and it seems unlikely that release of methane clathrates or its effect on the ocean composition would persist over the time of deposition of such thick stratigraphic intervals. An increase in biogenic methane production and recycling during early diagenesis in settings with high organic productivity and low sulfate content is another possible explanation for this trend (Hayes, 1983, 1994). Low S/C ratios in organic-rich shales in several Fennoscandian basins (Karhu, 1993; Melezhik et al., 1999b) might be related to low sulfate content in the ocean and in shallow-water environment after mixing with deep waters that had low sulfate content and were charged with reduced compounds.

Contrary to the view that supercontinent breakup might results in enhanced organic carbon burial through the formation of extensive shallow marine shelf areas (Des Marais, 1994; Hoffman et al., 1998), the opposite appears true for the end of the ca. 2.2–2.1 Ga carbon isotope excursion, insofar as the breakup of Kenorland followed the biogeochemical event. Similarly, the Paleoproterozoic record does not support arguments that high rates of organic matter burial due to high productivity and nutrient flux into semi-restricted basins led to either a local or global carbon isotope excursions (Melezhik et al., 1999a). Contrary to the proposed cause and effect relationship in the Neoproterozoic (Kaufman et al., 1997; Hoffman et al., 1998) and early Paleoproterozoic (Bekker et al., 2001a), the ca. 2.2–2.1 Ga positive carbon isotope excursion did not lead to known glaciation. Lastly, the biogeochemical events recorded in the Nash Fork Formation and its equivalents in Wyoming and around the world do not coincide with mantle plume activity, which occurs later (Puchtel et al., 1998; Hanski et al., 2001).

Event stratigraphy coupled with charted changes in the isotopic composition of the world ocean provides critical constraints on changing environments throughout Earth history. Results of these studies reaffirm our view that global tectonic processes ultimately drove the climatic and oceanographic changes, which led to the deposition of important mineral reserves.

11. Conclusions

1) The Nash Fork Formation was deposited after the Paleoproterozoic glacial epoch. Carbonates from the base of the Nash Fork Formation have remarkably high $\delta^{13}C$ values up to +28‰ whereas carbonates in the lower and middle parts have $\delta^{13}C$ values ranging between +6 and +8‰. Carbonates in the upper Nash Fork Formation above the carbonaceous shale have $\delta^{13}C$ values ranging between 0 and +2.5‰. This change in carbon isotope trend is similar to that observed in Fennoscandia where it is constrained between 2.11 and 2.06 Ga and is also marked by

organic-rich shales (Karhu, 1993). Based on the similar chemo- and lithostratigraphy of these successions, age constraints from Fennoscandia for the end of the carbon isotope excursion can be inferred for the depositional age of the Nash Fork Formation. These new age constraints conflict with the earlier proposed lithostratigraphic correlation of this unit with the Gordon Lake Formation, Huronian Supergroup, ON, and Randville Dolomite, Marquette Range Supergroup, MI (Houston et al., 1992). These age constraints also imply that the Upper Libby Creek Group including the Nash Fork Formation was deposited on a passive margin rather than in a foreland basin as was inferred earlier (Karlstrom et al., 1983) since it is significantly older than 1.78–1.74 Ga old volcanic arc that overrode the southern flank of the Wyoming Craton.

2) Sedimentary successions deposited at the end of the ca. 2.2–2.1 Ga carbon isotope excursion contain BIFs, Mn-rich lithologies, organic-rich shales with very low $\delta^{13}C_{org}$ values, phosphorites, and voluminous mafic volcanics. The stratified anoxic ocean that existed during the ca. 2.2–2.1 Ga carbon isotope excursion was overturned as new seaways opened and/or atmospheric and ocean temperatures rose as a result of voluminous volcanism during the Kenorland breakup. Deep waters enriched in P, Mn, Fe, and carbonate alkalinity with ^{13}C-depleted carbon isotope values were delivered to the shallow parts of the ocean and mixed with oxygenated waters. Mixing of deep and shallow waters led to precipitation of Fe and Mn oxides and phosphorites at the chemocline. High nutrient flux stimulated productivity led to high rates of organic carbon burial in localized areas.
3) Carbonates of the Slaughterhouse Formation, Sierra Madre, and the Whalen Group exposed in the Rawhide Creek area, Hartville Uplift, have highly positive $\delta^{13}C$ values, were deposited during the ca. 2.2–2.1 Ga carbon isotope excursion and correlate with the lower and middle Nash Fork Formation in the Medicine Bow Mountains. The areal extent of the carbonate passive margin platform that extended along the southern flank of the Wyoming Craton supports an open-marine depositional setting for these carbonates and thus a global rather than local signature for their highly positive carbon isotope systematics.
4) Carbonates of the Whalen Group from other localities in the Hartville Uplift and the Estes and Roberts Draw formations in the Black Hills have carbon isotope values close to 0‰, correlate with the upper Nash Fork Formation and postdate the ca. 2.2–2.1 Ga carbon isotope excursion.
5) Correlation between the Estes Formation, a rift succession on the eastern flank of the Wyoming Craton, and the upper Nash Fork Formation, deposited on the mature passive margin along the southern flank of the Wyoming Craton suggests that the two drowning events on the Nash Fork platform might be related to reactivation in response to this rifting event. The ocean opening on the eastern flank of the Wyoming Craton that is related to the final breakup of the Kenorland supercontinent occurred after the ca. 2.2–2.1 Ga positive carbon isotope excursion. Since the change in the carbon isotope trend straddles the second drowning event in the Nash Fork Formation, a temporal relationship exists between the final breakup of the Kenorland, relative sealevel rise, and the end of the carbon isotope excursion. A similar relationship has been recognized in Fennoscandia.

Acknowledgements

This project started when AB was an M.S. student at the University of Minnesota, Duluth, under the direction of Dick Ojakangas. Kevin Chamberlain provided helpful discussions on the tectonic setting and geochronology of the Snowy Pass Supergroup. Paul Graff, Jack Redden, Paul Sims, Warren Day, and Kevin Chamberlain helped in the field and shared their knowledge of geology of these areas. Discussions with Ed DeWitt on geology of the Black Hills are greatly

appreciated. Comments by Fred Read and Peter S. Dahl on an earlier version of the manuscript are greatly appreciated. H. Hofmann is gratefully acknowledged for sharing information and providing sample from the Hartville Uplift that led to our discovery of the carbon isotope excursion in this area. Don Rimstidt provided access to and helped with AAS work. Support came from the Department of Geology, University of Minnesota, Duluth; GSA and southeastern section of GSA; Colorado Scientific Society; and the Graduate School and Department of Geological Sciences, VPI and SU. JAK thanks the Geological Survey of Finland for permission to publish data produced in their laboratories. Funding for participation by AJK and isotopic analyses at the University of Maryland was provided by NSF grants EAR-96-14070 and EAR-98-17348. AB gratefully acknowledges financial support from PRF grant 37194-AC2 to H.D. Holland, Harvard University.

References

Äikäs, O., 1980. Uraniferous phosphorite and apatite-bearing gneisses in the Proterozoic of Finland. In: Proceedings of the International Uranium Symposium on the Pine Creek Geosyncline, pp. 675–681.

Akhmedov, A.M., 1990. Epochs of evaporization in the Paleoproterozoic of the Baltic Shield. Dokl. Akad. Nauk SSSR 312 (3), 698–702.

Akhmedov, A.M., Travin, L.V., Tikhomirova, M., 1996. Glacial and evaporate epochs in the early Proterozoic and interregional correlation. Reg. Geol. Metallogeny (5), 84–97.

Amelin, Y.V., Heaman, L.M., Semenov, V.S., 1995. U–Pb geochronology of layered intrusions in the eastern Blatic Shield: implications for the timing and duration of Paleoproterozoic continental rifting. Precambrian Res. 75, 31–46.

André, L., 1993. Age Rb–Sr Proterozoique inferieur du magmatisme continental du Groupe de la Lulua (Kasai, Zaire): Ses implications geodynamiques. Annales de la Société Géologique de Belgique 116 (1), 1–12.

Asmerom, Y., Jacobsen, S.B., Knoll, A.H., Butterfield, N.J., Swett, K., 1991. Strontium isotopic variations of Neoproterozoic seawater: implications for crustal evolution. Geochim. Cosmochim. Acta 55, 2883–2894.

Aspler, L.B., Chiarenzelli, J.R., 1998. Two Neoarchean supercontinents? Evidence from the Paleoproterozoic. Sedimentary Geol. 120, 75–104.

Awramik, S.M., Sprinkle, J., 1999. Proterozoic stromatolites: the first marine evolutionary biota. Historical Biol. 13, 241–253.

Baker, A.J., Fallick, A.E., 1989a. Evidence from the Lewisian limestone for isotopically heavy carbon in two-thousand-million-year-old seawater. Nature 337, 352–354.

Baker, A.J., Fallick, A.E., 1989b. Heavy carbon in two-billion-year-old marbles from Lofoten-Vesterålen, Norway: implications for the Precambrian carbon cycle. Geochim. Cosmochim. Acta 53, 1111–1115.

Balashov, Y.A., 1996. Geochronology of the early Proterozoic rocks of the Pechenga-Varzuga structure, Kola Peninsula. Petrology 4 (1), 3–25.

Ball, T.T., Farmer, G.L., 1991. Identification of 2.0 to 2.4 Ga Nd model age crustal material in the Cheyenne belt, northeastern Wyoming: implications for Proterozoic accretionary tectonics at the southern margin of the Wyoming Craton. Geology 19, 360–363.

Banerjee, D.M., 1971. Precambrian stromatolitic phosphorites of Udaipur, Rajasthan, India. Geol. Soc. Am. Bull. 82, 2319–2330.

Banerjee, D.M., Schidlowski, M., Arneth, J.D., 1986. Genesis of upper Proterozoic-Cambrian phosphorite deposits of India: isotopic inferences from carbonate fluorapatite, carbonate and organic carbon. Precambrian Res. 33, 239–253.

Barley, M.E., Pickard, A.L., Sylvester, P.J., 1997. Emplacement of a large igneous province as a possible cause of banded iron formation 2.45 billion years ago. Nature 385, 55–58.

Bekasova, N.B., Dudkin, O.B., 1982. Composition and nature of concretionary phosphorites from the early Precambrian of Pechenga (Kola Peninsula). Lithol. Mineral Resourc., 16(6), 625–630.

Bekker, A., 1998. Chemostratigraphy and climatostratigraphy of the Paleoproterozoic Snowy Pass Supergroup, Wyoming and its application for correlation with other sequences in North America. M.S. Thesis. University of Minnesota, Duluth, 104 pp.

Bekker, A., Eriksson, K.A., 2003. Paleoproterozoic drowned carbonate platform on the southeastern margin of the Wyoming Craton: a record of the Kenorland breakup. Precambrian Res. (in press).

Bekker, A., Karhu, J.A., Eriksson, K.A., 1997. Paleoenvironmental Changes at the end of the Paleoproterozoic Carbon Isotope Excursion ($\sim$2.06 Ga), Vol. 29, No. 6. GSA Annual Meeting. Abstract with Programs, 1997, p. 467.

Bekker, A., Eriksson, K.A., Kaufman, A.J., Karhu, J.A., Beukes, N.J., 1999. Paleoproterozoic Record of Biogeochemical Events and Ice Ages, Vol. 31, No. 7. GSA Annual Meeting. Abstract with Programs, 1999, p. 487.

Bekker, A., Kaufman, A.J., Karhu, J.A., Beukes, N.J., Swart, Q.D., Coetzee, L.L., Eriksson, K.A., 2001a. Chemostratigraphy of the Paleoproterozoic Duitschland Formation, South Africa: implications for coupled climate change and carbon cycling. Am. J. Sci. 301, 261–285.

Bekker, A., Master, S., Karhu, J.A., Verhagen, B.T., 2001b. Chemostratigraphy of the Paleoproterozoic Magondi

Supergroup, Zimbabwe. In: Proceedings of the 11th Ann. V. M. Goldschmidt Conference, Abst. 3772. LPI Contr.1088. Lunar and Planetary Institute, Houston (CD-ROM).

Boiko, V.L., Dobrokhotov, M.N., Esipchuk, K.E., Semenenko, N.P., Shcherbak, N.P., 1989. Lower Precambrian stratigraphy of the Ukraine Shield. In: Sokolov, B.S. (Ed.), Stratigraphy of the USSR. Lower Precambrian. Nedra, Moscow, pp. 194–257.

Bol, L.C.G.M., Nijland, T.G., Sauter, P.C.C., Jansen, J.B.H., Valley, J.W., 1995. Preservation of premetamorphic oxygen and carbon isotopic trends in granulite facies marbles from Rogaland, southwest Norway. Am. J. Sci. 295, 1179–1219.

Borshchevsky, Y.A., Borisova, S.L., Yudin, N.I., Medvedovskaya, N.I., Stepanova, T.I., Krasotov, Y.M., Popova, N.K., Voronina, Y.V., Belkov, E.I., 1982. Isotope characteristics of apatite–calcite associations of Slyudyanka Series, peri-Baykal, Abstracts. In: Proceedings of the Ninth All-Union Symposium on Stable Isotopes in Geochemistry, Moscow, pp. 421–423.

Bros, R., Stille, P., Gauthier-Lafaye, F., Weber, F., Clauer, N., 1992. Sm–Nd isotopic dating of Proterozoic clay material: an example from the Francevillian sedimentary series, Gabon. Earth Plan. Sci. Lett. 113, 207–218.

Buchan, K.L., Mortensen, J.K., Card, K.D., Percival, J.A., 1998. Paleomagnetism and U–Pb geochronology of diabase dyke swarms of Minto block Superior Province, Quebec, Canada. Can. J. Earth Sci. 35, 1054–1069.

Bühn, B., Stanistreet, I.G., 1997. Insight into enigma of Neoproterozoic manganese and iron formations from the perspective of supercontinent breakup and assembly. In: Nicholson, K., Hein, J.R., Bühn, B., Dasgupta, S. (Eds.), Manganese Mineralization: Geochemistry and Mineralogy of Terrestrial and Marine Deposits. Geol. Soc. Spec. Publ. 119, London, 1997, pp. 81–90.

Buick, R., Des Marais, D.J., Knoll, A.H., 1995. Stable isotope compositions of carbonates from the Mesoproterozoic Bangemall Group, northwestern Australia. Chem. Geol. 123, 153–171.

Buick, I.S., Uken, R., Gibson, R.L., Wallmach, T., 1998. High-$\delta^{13}C$ Paleoproterozoic carbonates from the Transvaal Supergroup, South Africa. Geology 26, 875–878.

Burdett, J.W., Grotzinger, J.P., Arthur, M.A., 1990. Did major changes in the stable-isotope composition of Proterozoic seawater occur? Geology 18, 227–230.

Cadman, A.C., Heaman, L.M., Tarney, J., Wardle, R., Krogh, T.E., 1993. U–Pb geochronology and geochemical variation within two Proterozoic mafic dyke swarms, Labrador. Can. J. Earth Sci. 30, 1490–1504.

Canfield, D.E., 1998. A new model for Proterozoic ocean chemistry. Nature 396, 450–453.

Canfield, D.E., Raiswell, R., 1991. Carbonate precipitation and dissolution: its relevance to fossil preservation. In: Allison, P.A., Briggs, D.E.G. (Eds.), Taphonomy: Releasing the Data Locked in the Fossil Record. Plenum Press, London, pp. 411–453.

Canfield, D.E., Raiswell, R., 1999. The evolution of the secular cycle. Am. J. Sci. 299, 697–723.

Chamberlain, K.R., 1998. Medicine Bow Orogeny: timing of deformation and model of crustal structure produced during continent-arc collision, ca. 1.78 Ga, southeastern Wyoming. Rocky Mnt. Geol. 33 (2), 259–277.

Cook, P., 1992. Phosphogenesis around the Proterozoic–Phanerozoic transition. J. Geol. Soc. London 149, 615–620.

Corfu, F., Andrews, A., 1986. A U–Pb age for mineralized Nipissing diabase, Gowganda, Ontario. Can. J. Earth Sci. 23, 107–112.

Cornell, D.H., Schütte, S.S., Eglington, B.L., 1996. The Ongeluk basaltic andesite formation in Griqualand West, South Africa: submarine alteration in a 2222 Ma Proterozoic sea. Precambrian Res. 79, 101–123.

Cox, D.M., Frost, C.D., Chamberlain, K.R., 2000. 2.01-Ga Kennedy dike swarm, southeastern Wyoming: record of a rifted margin along the southern Wyoming province. Rocky Mnt. Geol. 35 (1), 7–30.

Crichton, J.G., Condie, K.C., 1993. Trace elements as source indicators in cratonic sediments: a case study from the Paleoproterozoic Libby Creek Group, southeastern Wyoming. J. Geol. 101, 319–332.

Dahl, P.S., Frei, R., 1998. Step-leach Pb–Pb dating of inclusion-bearing garnet and staurolite, with implications for early Proterozoic tectonism in the Black Hills collisional orogen, South Dakota, United States. Geology 26, 111–114.

Dahl, P.S., Holm, D.K., Gardner, E.T., Hubacher, F.A., Foland, K.A., 1999. New constraints on the timing of early Proterozoic tectonism in the Black Hills (South Dakota), with implications for docking of the Wyoming province with Laurentia. Geol. Soc. Am. Bull. 111 (9), 1335–1349.

Davis, D.J., 1997. U–Pb zircon and rutile ages from granulite xenoliths in the Slave province: evidence for mafic magmatism in the lower crust coincident with Proterozoic dike swarms. Geology 25, 343–346.

Davis, D.W., Hirdes, W., Schaltegger, U., Nunoo, E.A., 1994. U–Pb age constraints on deposition and provenance of Birimian and gold-bearing Tarkwaian sediments in Ghana, West Africa. Precambrian Res. 67, 89–107.

Day, W.C., Sims, P.K., Snyder, G.L., Wilson, A.B., Klein, T.L., 1999. Peterman, Z.E., Futa, K., Zartman, R.E. (Eds.), Geologic Map of Precambrian Rocks, Rawhide Buttes West Quadrangle and Part of Rawhide Buttes East Quadrangle, Hartville Uplift, Goshen and Niobrara Counties, Wyoming with a section on Geochronology. US Department of the Interior US Geol. Surv. Misc. Invest. Ser. I-2635, 1999, pp. 1–14.

Des Marais, D.J., 1994. Tectonic control of the crustal organic carbon reservoir during the Precambrian. Chem. Geol. 114, 303–314.

DeWitt, E., Redden, J.A., Wilson, A.B., Buscher, D., 1986. Mineral resource potential and geology of the Black Hills National Forest, South Dakota and Wyoming. US Geol. Surv. Bull. No. 1580, 135 pp.

DeWitt, E., Redden, J.A., Buscher, D., Wilson, A.B., 1989. Geologic map of the Black Hills area, South Dakota and

Wyoming. US Department of the Interior US Geol. Surv. Misc. Invest. Series Map I–1910.

Dickens, G.R., 2001. On the fate of past gas: What happens to methane released from a bacterially mediated gas hydrate capacitor? Geochem. Geophys. Geosyst. 2. Paper No. 2000GC000131.

Dickens, G.R., Castillo, M.M., Walker, J.C.G., 1997. A blast of gas in the latest Paleocene: simulating first-order effects of massive dissociation of oceanic methane hydrate. Geology 25, 259–262.

Divis, A.F., 1976. Geology and geochemistry of Sierra Madre Range, Wyoming. Quart. Colorado School Mines 71 (3), 127.

Donnelly, T.H., Shergold, J.H., Southgate, P.N., Barnes, C.J., 1990. Events leading to global phosphogenesis around the Proterozoic/Cambrian boundary. In: Notholt, A.J.G., Jarvis, I. (Eds.), Phosphorite Research and Development. Geol. Soc. Spec Publ. 52, 1990, pp. 273–287.

Doyen, L., 1973. The Manganese ore deposit of Kisenge-Kamata (western Katanga). In: Amstutz, G.C., Bernard, A.J. (Eds.), Mineralogical and Sedimentological Aspects of the Primary Ore. Proceedings of the Eighth International Sedimentological Congress on Ores in Sediments. Springer, Heidelberg, 1973, pp. 93–100.

Doyen, L., 1974. The manganese ore deposit of Kisenge–Kamata–Kapolo (western Katanga–Shaba–Zaire). In: Geochemical Composition of the Primary Carbonate Ore, Vol. 3. Proceedings of the Fourth IAGOD Symposium on Problems of Ore Deposition, Varna, Bulgaria, pp. 122–128.

Dzigbodi-Adjimah, K., Sogbor, S.F., 1993. The mineralogy and genetic significance of the manganese carbonate ore at Nsuta, Ghana. In: Tsidzi, K.E.N. (Ed.), Proceedings of the National Seminar on Current Developments in the Minerals Industry of Ghana. University of Science and Technology and Institute of Mining and Mineral Engineering (IMME), Kumasi, Ghana, pp. 25–32.

El Tabakh, M., Grey, K., Pirajno, F., Schreiber, B.C., 1999. Pseudomorphs after evaporitic minerals interbedded with 2.2 Ga strmatolites of the Yerriba basin, western Australia: origin and significance. Geology 27 (10), 871–874.

Fenton, C.L., Fenton, M.A., 1939. Precambrian and Paleozoic algae. Geol. Soc. Am. Bull. 50, 89–126.

Feybesse, J.L., Johan, V., Triboulet, C., Guerrot, C., Mayaga-Mikolo, F., Bouchot, V., Eco N'dong, J., 1998. The west-central African belt: a model of 2.5–2.0 Ga accretion and two-phase orogenic evolution. Precambrian Res. 87, 161–216.

Frank, T.D., Lyons, T.W., 2000. The integrity of $\delta^{18}O$ records in Precambrian carbonates: a Mesoproterozoic case study. In: Grotzinger, J.P., James, N.P. (Eds.), Carbonate Sedimentation and Diagenesis in the Evolving Precambrian World. SEPM Spec. Publ. 67, 2000, pp. 315–326.

Gauthier-Lafaye, F., Weber, F., 1989. The Francevillian (lower Proterozoic) uranium ore deposits of Gabon. Econ. Geol. 84, 2267–2285.

Gehör, S., 1994. REE distribution in the phosphorite bands within the Paleoproterozoic Tuomivaara and Pahtavaara iron-formations, central and northern Finland. In: Nironen, M., Kähkönen, Y. (Eds.), Geochemistry of Proterozoic Supracrustal Rocks in Finland. Geol. Survey Finland Spec. Pap. 19, Espoo, pp. 71–84.

Golubev, A.I., Akhmedov, A.M., Galdobina, L.P., 1984. Geochemistry of the Lower Proterozoic Black Shale Complexes from the Karelia-Kola region. Nauka, Leningrad, p. 192.

Gorokhov, I.M., Semikhatov, M.A., Baskakov, A.V., Kutyavin, E.P., Melnikov, N.N., Sochava, A.V., Turchenko, T.L., 1995. Sr isotopic composition in Riphean, Vendian, and Lower Cambrian carbonates from Siberia. Str. Geol. Cor. 3, 1–28.

Gorokhov, I.M., Kuznetsov, A.B., Melezhik, V.A., Konstantinova, G.V., Melnikov, N.N., 1998. Sr isotopic composition in the upper Jatulian (early Proterozoic) dolomites of the Tulomozero Formation, southeastern Karelia. Dokl. Akad. Nauk SSSR 360 (4), 533–536.

Grotzinger, J.P., Knoll, A.H., 1995. Anomalous carbonate precipitates: is the Precambrian the key to the Permian? Palaios 10, 578–596.

Guliy, V.N., 1995a. Main features of composition and origin of apatite deposits in metamorphic rocks of the Aldan Shield, Siberia, Russian Federation. Trans. Inst. Min. Metall. Sect. B 104, B171–B178.

Guliy, V.N., 1995b. Metasedimentary apatite deposits of the Birikeen area, Aldan Shield. Lithol. Mineral Resourc. 30 (6), 545–555.

Gutzmer, J., Beukes, N.J., 1996. Karst-hosted freshwater Paleoproterozoic manganese deposits, Postmasburg, South Africa. Econ. Geol. 91, 1435–1454.

Hallock, P., Schlager, W., 1986. Nutrient excess and the demise of coral reefs and carbonate platforms. Palaios 1, 389–398.

Hanski, E., Huhma, H., Rastas, P., Kamenetsky, V.S., 2001. The Paleoproterozoic komatiite-picrite association of Finnish Lapland. J. Petr. 42 (5), 855–876.

Hayes, J.M., 1983. Geochemical evidence bearing on the origin of aerobiosis, a speculative interpretation. In: Schopf, J.W. (Ed.), The Earth's Earliest Biosphere: Its Origin and Evolution. Princeton University Press, Princeton, NJ, pp. 93–134.

Hayes, J.M., 1994. Global methanotrophy at the Archean–Proerozoic transition. In: Bengston, S. (Ed.), Proc. Nobel Symp. 84. Early Life on Earth. Columbia University Press, New York, pp. 220–236.

Hayes, J.M., Strauss, H., Kaufman, A.J., 1999. The abundance of ^{13}C in marine organic matter and isotopic fractionation in the global biogeochemical cycle of carbon during the past 800 Ma. Chem. Geol. 161, 103–125.

Heaman, L.M., 1997. Global mafic volcanism at 2.45 Ga: remnants of an ancient large igneous province? Geology 25, 299–302.

Hein, J.R., Bolton, B.R., 1993. Composition and origin of the Moanda manganese deposit, Gabon. In: Proceedings of the 16th International Colloquium on African Geology. Extended Abstracts. Geological Survey and Mines Department of Swaziland, Ezulwini, Swaziland, pp. 150–152.

Hein, J.R., Bolton, B.R., Nziengui, P., McKirdy, D., Frakes, L., 1989. Chemical, isotopic and lithologic associations within the Moanda manganese deposit, Gabon. In: Proceedings of the 28th International Geological Congress, Abstracts, Washington, DC, pp. 2–46.

Hein, J.R., Fan, D., Ye, J., Liu, T., Yeh, H.-W., 1999. Composition and origin of early Cambrian Tiantaishan phosphorite-Mn carbonate ores, Shaanxi Province, China. Ore Geol. Rev. 15, 95–134.

Hirdes, W., Davis, D.W., 1998. First U–Pb zircon age of extrusive volcanism in the Birimian Supergroup of Ghana/West Africa. J. Afr. Earth Sci. 27 (2), 291–294.

Hoffman, P.F., Kaufman, A.J., Halverson, G.P., Schrag, D.P., 1998. A Neoproterozoic Snowball Earth. Science 281, 1342–1346.

Hofmann, H.J., Davidson, A., 1998. Paleoproterozoic stromatolites, Hurwitz Group, Quartzite Lake area, Northwest Territories, Canada. Can. J. Earth Sci. 35, 280–289.

Hofmann, H.J., Snyder, G.L., 1985. Archean stromatolites from the Hartville Uplift, eastern Wyoming. Geol. Soc. Am. Bull. 96, 842–849.

Houston, R.S., 1993. Late Archean and Paleoproterozoic geology of southeastern Wyoming. In: Snoke, A.W., Steidtmann, J.R., Roberts, S.M. (Eds.), Geology of Wyoming. Geological Survey of Wyoming Memoir, vol. 5, pp. 78–116.

Houston, R.S., Graff, P.J., 1995. Geologic map of Precambrian rocks of the Sierra Madre, Carbon County, Wyoming, and Jackson and Routt Counties, Colorado. US Department of the Interior US Geol. Surv., Misc. Invest. Ser. I-2452.

Houston, R.S., Lanthier, L.R., Karlstrom, K.E., Sylvester, G., 1981. Paleoproterozoic diamictite of southern Wyoming. In: Hambrey, M.J., Harland, W.B. (Eds.), Earth's Pre-Pleistocene Glacial Record. Cambridge University Press, New York, pp. 795–799.

Houston, R.S., Karlstrom, K.E., Graff, P.J., Flurkey, A.J., 1992. New stratigraphic subdivisions and redefinition of subdivisions of Late Archean and Paleoproterozoic metasedimentary and metavolcanic rocks of the Sierra Madre and Medicine Bow Mountains, southern Wyoming. US Geological Survey Prof. Pap. 1520, 50 pp.

Ingall, E.D., Jahnke, R., 1994. Evidence for enhanced phosphorus regeneration from marine sediments overlain by oxygen depleted waters. Geochim. Cosmochim. Acta 58 (11), 2571–2575.

Isley, A.E., 1995. Hydrothermal plumes and the delivery of iron to banded iron formation. J. Geol. 103, 169–185.

Isley, A.E., Abbott, D.H., 1999. Plume-related mafic volcanism and the deposition of banded iron formation. J. Geophys. Res. 104 (B7), 15461–15477.

Kah, L.C., 2000. Depositional $\delta^{18}O$ signatures in Proterozoic dolostones: constraints on seawater chemistry and early diagenesis. In: Grotzinger, J.P., James, N.P. (Eds.), Carbonate Sedimentation and Diagenesis in the Evolving Precambrian World. SEPM Spec. Publ. 67, 2000, pp. 345–360.

Kanygin, L.I., Kirikilitsa, S.I., Krivonos, V.P., Levenshteyn, M.L., Polunovsky, R.M., Porokhnenko, A.F., Kharagezov, M.K., 1969. On finding perspectives of metamorphogenic deposits of manganese and phosphate in Precambrian carbonate units of peri-Azov. Geol. J. 29 (4), 146–147.

Karhu, J.A., 1993. Paleoproterozoic evolution of the carbon isotope ratios of sedimentary carbonates in the Fennoscandian Shield. Geol. Surv. Finland Bull. 371, Espoo, 87 pp.

Karhu, J.A., Holland, H.D., 1996. Carbon isotopes and the rise of atmospheric oxygen. Geology 24 (10), 867–870.

Karlstrom, K.E., Houston, R.S., 1984. The Cheyenne belt: analysis of a Proterozoic suture in southern Wyoming. Precambrian Res. 25, 415–446.

Karlstrom, K.E., Flurkey, A.J., Houston, R.S., 1983. Stratigraphy and depositional setting of the Proterozoic Snowy Pass Supergroup, southeastern Wyoming: Record of a Paleoproterozoic Atlantic-type cratonic margin. Geol. Soc. Am. Bull. 94, 1257–1274.

Kaufman, A.J., Knoll, A.H., 1995. Neoproterozoic variations in the C-isotopic composition of seawater: stratigraphic and biogeochemical implications. Precambrian Res. 73, 27–49.

Kaufman, A.J., Knoll, A.H., Narbonne, G.M., 1997. Isotopes, ice ages, and terminal Proterozoic Earth history. Nat. Acad. Sci. Proc. 94, 6600–6605.

Kennedy, M.J., Christie-Blick, N., Sohl, L., 2001. Are Proterozoic cap carbonates and isotopic excursions: a record of gas hydrate destabilization following Earth's coldest intervals? Geology 29 (5), 443–446.

Kirkham, R.V., Roscoe, S.M., 1993. Atmospheric evolution and ore deposit formation. Resource. Geol. Spec. Iss. No. 15, 1–17.

Klein, C., Beukes, N.J., 1993. Sedimentology and geochemistry of the glaciogenic late Proterozoic Rapitan iron formation in Canada. Econ. Geol. 88, 542–565.

Knoll, A.H., Hayes, J.M., Kaufman, A.J., Swett, K., Lambert, I.B., 1986. Secular variations in carbon isotope ratios from Upper Proterozoic successions of Svalbard and East Greenland. Nature 321, 832–838.

Knoll, A.H., Bambach, R.E., Canfield, D.E., Grotzinger, J.P., 1996. Comparative Earth history and late Permian mass extinction. Science 273, 452–457.

Koneva, A.A., Makrygina, V.A., Reznitskii, L.Z., 1998. Gondites in metamorphic sequences of the Baikal Region. Lithol. Mineral Resourc. 33 (1), 82–91.

Kotov, A.B., Salnikova, E.B., Reznitskii, L.Z., Natman, A., Kovach, V.P., Zagornaya, N.Y., Belyaevskii, N.A., 2000. Age and sources of deeply metamorphosed supracrustal deposits of the Slyudyanka crystalline complex (southern peri-Baykal). In: Negrutza, T.F., Negrutza, V.Z. (Eds.), General Issues of Precambrian Subdivision. Materials of 3d All-Union Conference. Geological Institute of the Kola Science Centre, Apatity, pp. 124–125.

Krapez, B., Martin, D.M., 1999. Sequence stratigraphy of the Paleoproterozoic Nabberu Province of western Australia. Aust. J. Earth Sci. 46, 89–103.

Kravchenko, G.L., 1993. Manganese garnet from graphitic gneisses of West Priazov. Geologicheskii Zhurnal (1), 24–30.

Krogh, T.E., Davis, D.W., Corfu, F., 1984. Precise U–Pb zircon and badelleyite ages for the Sudbury area. In: Pye, E.G., Naldrett, A.J., Giblin, P.E. (Eds.), The geology and ore deposits of the Sudbury structure. Ontario Geol. Surv. Spec., vol. 1, pp. 431–446.

Krogh, T.E., Kamo, S.L., Bohor, B.F., 1996. Shock metamorphosed zircons with correlated U–Pb discordance and melt rocks with concordant protolith ages indicate an impact origin for the Sudbury structure. Earth processes: reading the isotopic code. Geophys. Monograph 95. Am Geophys Union, pp. 343–353.

Kulish, E.A., 1970. Behaviour of oxygen in the Archean Aldanian atmosphere. Dokl. Akad. Nauk SSSR 191 (4), 921–923.

Kulish, E.A., Yatsenko, G.M., Kulish, L.I., Yanchuk, Y.A., Rosikhina, A.I., Kostyuchenko, V.S., 1988. Metamorphogenic Manganese Mineralization in Archean Complexes of Pobuzh'ya (Ukrainian Shield), Protsessy i Zakonomernosti Metamorfogennogo Rudoobrazovaniia. Naukova Dumka, Kiev, pp. 125–134.

Kump, L.R., Kasting, J.F., Barley, M.E., 2000. The rise of atmospheric oxygen and the "upside down" Archean mantle. Geochem. Geophys. Geosyst., Vol. 2. Paper No. 2000GC000114.

Laajoki, K., Saikkonen, R., 1977. On the geology and geochemistry of the Precambrian iron formations in Väyrylänkylä, South Puolanka area, Finland. Geol. Surv. Finland Bull. 292, 1–137.

Lanyon, R., Black, L.P., Seitz, H.-M., 1993. U–Pb zircon dating of mafic dykes and its application to the Proterozoic geological history of the Vestfold Hills, East Antarctica. Contrib. Mineral. Petrol. 115, 184–203.

Lazar, B., Erez, J., 1990. Extreme ^{13}C depletions in seawater-derived brines and their implications for the past geochemical carbon cycle. Geology 18, 1191–1194.

Lazur, Y.M., Kazantsev, V.A., Ermilov, V.V., 1981. Manganiferous sulfide mineralization in Proterozoic carbonaceous deposits of KMA district in Russian. Dokl. Akad. Nauk SSSR 256 (3), 677–680.

Leclerc, J., Weber, F., 1980. Geology and genesis of the Moanda manganese deposits, Republic of Gabon. In: Varentsov, I.M., Grasselly, G. (Eds.), Geology and Geochemistry of Manganese, E. Schweizerbart'sche Verlagsbuchhandlung (Nagele U. Obermiller), Stuttgart, pp. 89–109.

Lindsay, J.F., Brasier, M.D., 2000. A carbon isotope reference curve for c. 1700 to 1575 Ma, McArthur and Mount Isa Basins, northern Australia. Precambrian Res. 99, 271–308.

Lindsay, J.F., Brasier, M.D., 2002. Did global tectonics drive early biosphere evolution? Carbon isotope record from 2.6 to 1.9 Ga carbonates of western Australian basins. Precambrian Res. 114, 1–34.

Lobzova, R.V., Esikov, A.D., 1981. On Carbon Sources for the Origin of Graphite Deposits in Light of Isotopic Data. Materials of the All-Union Conference on Carbon Geochemistry. Nauka, Moscow, pp. 63–64.

Maheshwari, A., Sial, A.N., Chittora, V.K., 1999. High-$\delta^{13}C$ Paleoproterozoic carbonates from the Aravalli Supergroup, western India. Int. Geol. Rev. 41, 949–954.

Marmo, J.S., 1992. The lower Proterozoic Hokkalampi paleosol in North Karelia, eastern Finland. In: Schidlowski, M., Golubic, S., Kimberly, M.M., Trudinger, P.A. (Eds.), Early Organic Evolution: Implications for Mineral and Energy Resources. Springer, Berlin, pp. 41–66.

Martin, D.M., Li, Z.X., Nemchin, A.A., Powell, C.M., 1998. A pre-2.2 Ga age for giant hematite ores of the Hamersley Province Australia? Econ. Geol. 93, 1084–1090.

Master, S., 1991. Stratigraphy, tectonic setting, and mineralization of the early Proterozoic Magondi Supergroup, Zimbabwe: a review. EGRU Information Circular 238, Johannesburg, 75 pp.

Master, S., Verhagen, B.T., Duane, M.J., 1990. Isotopic signatures of continental and marine carbonates from the Magondi Belt, Zimbabwe: implications for the global carbon cycle at 2,0 Ga. In: Proceedings of the 23rd Earth Sci. Cong. Geol. Soc. S. Afr. Abstr., Cape Town, pp. 346–348.

Master, S., Verhagen, B.T., Bassot, J.P., Beukes, N.J., Lemoine, S., 1993. Stable isotopic signatures of Paleoproterozoic carbonate rocks from Guinea, Senegal, South Africa and Zimbabwe: constrains on the timing of the ca. 2 Ga "Lomagundi" $\delta^{13}C$ excursion, Symposium: Early Proterozoic Geochemical and Structural Constraints—Metallogeny. Publication Occasionnelle 1993/23, Dacar, Sénégal, pp. 38–41.

McCombs, J.A., Dahl, P.S., Hamilton, M.A., Stern, R.A., 2001. Ion microprobe (SHRIMP U–Pb) study of zircon geochronology in Archean basement lithologies, Black Hills, South Dakota. GSA Annual Meeting, Abstract with Programs, p. A143.

Melezhik, V.A., Fallick, A.E., 1996. A widespread positive $\delta^{13}C_{carb}$ anomaly at around 2.33–2.06 Ga on the Fennoscandian Shield: a paradox? Terra Nova 8, 141–157.

Melezhik, V.A., Predovsky, A.A., 1982. Geochemistry of the Early Proterozoic Lithogenesis (Using the Northeast of the Baltic Shield as an Example). Nauka, Leningrad, p. 208.

Melezhik, V.A., Fallick, A.E., Makarikhin, V.V., Lyubtsov, V.V., 1997a. Links between Paleoproterozoic palaeogeography and rise and decline of stromatolites: Fennoscandian Shield. Precambrian Res. 82, 311–348.

Melezhik, V.A., Fallick, A.E., Clark, T., 1997b. Two billion-year-old isotopically heavy carbon: evidence from the Labrador Trough, Canada. Can. J. Earth Sci. 34 (3), 271–285.

Melezhik, V.A., Fallick, A.E., Medvedev, P.V., Makarikhin, V.V., 1999a. Extreme $\delta^{13}C_{carb}$ enrichment in ca. 2.0 Ga magnesite–stromatolite–dolomite–'red beds' association in a global context: a case for the world-wide signal enhanced by a local environment. Earth Sci. Rev. 48, 71–120.

Melezhik, V.A., Fallick, A.E., Filippov, M.M., Larsen, O., 1999b. Karelian shungite—an indication of 2.0-Ga-old

metamorphosed oil-shale and generation of petroleum: geology, lithology and geochemistry. Earth Sci. Rev. 47, 1–40.

Mirota, M.D., Veizer, J., 1994. Geochemistry of Precambrian Carbonates. IV. Aphebian Albanel Formations, Quebec, Canada. Geochim. Cosmochim. Acta 58, 1735–1745.

Montañez, I.P., Banner, J.L., Osleger, D.A., Borg, L.E., Bosserman, P.J., 1996. Integral Sr isotope variations and sea-level history of Middle to Upper Cambrian platform carbonates: implications for the evolution of Cambrian seawater $^{87}Sr/^{86}Sr$. Geology 24 (10), 917–920.

Mücke, A., Dzigbodi-Adjimah, K., Annor, A., 1999. Mineralogy, petrology, geochemistry and genesis of the Paleoproterozoic Birimian manganese-formation of Nsuta/Ghana. Min. Dep. 34, 297–311.

Nayak, V.K., 1980. The manganese ores of Kajlidongri, District Jhabua, Madhya Pradesh, India. In: Varentsov, I.M., Grasselly, G. (Eds.), Geology and Geochemistry of Manganese, E. Schweizerbart'sche Verlagsbuchhandlung (Nagele U. Obermiller), Stuttgart, pp. 265–277.

Nikitina, A.P., Shchipanskiy, A.A., 1987. Phosphorus resources in the early Proterozoic deposits of Belgorod district, KMA. Izvestiya Akademii Nauk SSSR, Seriya Geologicheskaya (2), 113–124.

Ojakangas, R.W., 1997. Correlative sequence within the Marquette Range Supergroup (Michigan) and the Huronian Supergroup (Ontario); Glaciogenics, paleosols, and orthoquartzites (Abs), 43rd Inst. Lake Superior Geol., pp. 47–48.

Paakola, J., 1971. The volcanic complex and associated manganiferous iron formation of the Porkonen–Pahtavaara area in Finnish Lapland. Bull. Com. Geol. Finl. N. 247, 82.

Pavlov, V.A., Cherdakov, V.I., Komarov, P.V., 1987. Mineralogic-geochemical peculiarities of rocks and ores in iron-bearing deposits of the southern Aldan. Geology Ore Deposits 5, 75–83.

Ponomarenko, A.I., 1973. Rhodonite-spessartine rocks of the Anabar massif. Dokl. Akad. Nauk SSSR 212 (6), 1426–1429.

Premo, W.R., Van Schmus, W.R., 1989. Zircon geochronology of Precambrian rocks in southeastern Wyoming and northern Colorado. In: Grambling, J.A., Tewksbury, B.J. (Eds.), Proterozoic Geology of the Southern Rocky Mountains. Geol. Soc. Am. Spec. Pap., vol. 235, pp. 1–12.

Prilutzky, R.E., Suslova, S.N., Nalivkina, Y.B., 1992. Reconstruction of environmental conditions of early Proterozoic carbonate deposits of the Ukrainian and Baltic Shields based on isotopic studies. Lithol. Mineral Deposits 5, 76–88.

Puchtel, I.S., Arndt, N.T., Hofmann, A.W., Haase, K.M., Kröner, A., Kulikov, V.S., Kilikova, V.V., Garbe-Schönberg, C.-D., Nemchin, A.A., 1998. Petrology of mafic lavas within the Onega plateau, central Karelia: evidence for 2.0 Ga plume-related continental crustal growth in the Baltic Shield. Contr. Mineral. Petrol. 130, 134–153.

Redden, J.A., 1980. Geology and uranium resources in Precambrian conglomerates of Nemo area, Black Hills, South Dakota: US DOE Natl. Uranium Resource Evaluation Report GJBX 127, No. 80, 1980, p. 147.

Redden, J.A., 1981. Summary of the geology of the Nemo area. In: Rich, F.J. (Ed.), Geology of the Black Hills, South Dakota and Wyoming. Geol. Soc. Am. Guidebook. Rocky Mountain Section, Annual Meeting, Rapid City, SD, 1981, pp. 193–210.

Redden, J.A., Peterman, Z.E., Zartman, R.E., DeWitt, E., 1990. U–Th–Pb geochronology and preliminary interpretation of Precambrian tectonic events in the Black Hills, South Dakota. In: Lewry, J.F., Stauffer, M.R. (Eds.), The Early Proterozoic Trans-Hudson Orogen of North America. Geol. Ass. Canada Spec. Pap. 37, 1990, pp. 229–251.

Reitsema, R.H., 1980. Dolomite and nahcolite formation in organic rich sediments: isotopically heavy carbonates. Geochim. Cosmochim. Acta 44, 2045–2049.

Reznitsky, L.Z., Vasil'ev, E.P., Vishnyakov, V.N., 1976. First finding of gondites in the Precambrian of the southern peri-Baikal. Dokl. Akad. Nauk SSSR 229 (5), 1195–1197.

Reznitsky, L.Z., Fefelov, N.N., Vasil'ev, E.P., Zarudneva, N.V., Nekrasova, E.A., 1998. Isotopic composition of lead from metaphosphorites and problem of the Slyudyanka Group age, the southern Baykal–western Khamar Daban Region. Lithol. Mineral Resourc. 33 (5), 432–441.

Rohon, M.-L., et al., 1993. Aphebian mafic-ultramafic magmatism in the Labrador Trough (New Quebec): its age and the nature of its mafic source. Can. J. Earth Sci. 30, 1582–1593.

Roscoe, S.M., Card, K.D., 1993. The reappearance of the Huronian in Wyoming: rifting and drifting of ancient continents. Can. J. Earth Sci. 30, 2475–2480.

Roy, S., 1980. Manganese ore deposits of India. In: Varentsov, I.M., Grasselly, G. (Eds.), Geology and Geochemistry of Manganese, E. Schweizerbart'sche Verlagsbuchhandlung (Nagele U. Obermiller), Stuttgart, pp. 237–264.

Rozen, O.M., Zlobin, V.L., Syngaevskiy, E.D., 1990. Metamorphic carbonate rocks of granulite complex of the Anabar Shield: peculiarities of primary composition and sedimentation. Lithol. Mineral Deposits 25(6), 72–81.

Rozen, O.M., Condie, K.C., Natapov, L.M., Nozhkin, A.D., 1994. Archean and early Proterozoic evolution of the Siberian Craton: a preliminary assessment. In: Condie, K.C. (Ed.), Archean Crustal Evolution. Elsevier, Amsterdam, pp. 411–459.

Rundqvist, D.V., Mitrofanov, F.P., 1993. Precambrian Geology of the USSR. Developments in Precambrian Geology, vol. 9. Elsevier, Amsterdam, p. 528.

Russell, J.R., 1992. Investigation of the potential of Pb/Pb radiometric dating for the direct age determination of carbonates. D. Phil. (unpublished) Thesis. University of Oxford, Oxford.

Salop, L.I., 1982. Geologic Development of the Earth in Precambrian. Nedra, Leningrad, p. 343.

Schidlowski, M., Todt, W., 1998. The Proterozoic Lomagundi carbonate province as paragon of a ^{13}C-enriched carbonate facies: geology, radiometric age and geochemical significance, Vol. 43. Chinese Sci. Bull., Abst. ICOG-9, Beijing, p. 114.

Schidlowski, M., Eichmann, R., Junge, C.E., 1976. Carbon isotope geochemistry of the Precambrian Lomagundi carbonate province, Rhodesia. Geochim. Cosmochim. Acta 40, 449–455.

Schipansky, A.A., Bogdanova, S.V., 1996. The Sarmatian crustal segment: Precambrian correlation between the Voronezh Massif and the Ukrainian Shield across the Dniepr-Donets Aulacogen. Tectonophysics 268, 109–125.

Schreiber, U.M., Eriksson, P.G., 1992. An early Paleoproterozoic braid-delta system in the Pretoria Group, Transvaal Sequense, South Africa. J. Afr. Earth Sci. 15, 111–125.

Semikhatov, M.A., Raaben, M.E., 1994. Dynamics of the global diversity of Proterozoic stromatolites. Article I: Northern Eurasia, China, and India. Stratigraphy Geol. Correlation 2, 492–513.

Semikhatov, M.A., Raaben, M.E., 1996. Dynamics of the global diversity of Proterozoic stromatolites. Article 2: Africa, Australia, North America, and general synthesis. Stratigraphy Geol. Correlation 4 (1), 24–50.

Semikhatov, M.A., Raaben, M.E., Sergeev, V.N., Veis, A.F., Artemova, O.V., 1999. Biotic events and positive δC_{carb} anomaly at 2.3–2.06 Ga. Stratigraphy Geol. Correlation 7 (5), 413–436.

Shields, G.A., Brasier, M.D., Stille, P., Dorjnamjaa, D., 2002. Factors contributing to high $\delta^{13}C$ values in Cryogenian limestones of western Mongolia. Earth Plan. Sci. Lett. 196, 99–111.

Shnyukov, E.F., Orlovsky, G.N., 1980. Manganese ores of the Ukrainian SSR. In: Varentsov, I.M., Grasselly, G. (Eds.), Geology and Geochemistry of Manganese, E. Schweizerbart'sche Verlagsbuchhandlung (Nagele U. Obermiller), Stuttgart, pp. 393–402.

Sial, A.N., Ferrerira, V.P., Dealmeida, A.R., Romano, A.W., Parente, C.V., Dacosta, M.L., Santos, V.H., 2000. Carbon isotope fluctuations in Precambrian carbonate sequences of several localities in Brazil. Ann. Acad. Bras. Ci. 72 (4), 539–558.

Sidorenko, A.V., Borshchevsky, Y.A., 1977. General tendencies in evolution of carbonate isotopic composition in the Precambrian and Phanerozoic. Dokl. Akad. Nauk SSSR 234 (4), 892–895.

Sidorenko, A.V., Borshchevsky, Y.A., Sidorenko, S.A., Ustinov, V.A., Popova, N.K., 1972. Isotopic composition of carbon from Precambrian metamorphic rocks. Dokl. Akad. Nauk SSSR 206 (2), 463–466.

Simonson, B.M., Hassler, S.W., 1996. Was the deposition of large Precambrian Iron Formations linked to major marine transgressions? J. Geol. 104, 665–676.

Sims, P.K., 1995. Archean and early Proterozoic tectonic framework of north-central United States and adjacent Canada. US Geol. Surv. Bull 1904-T, 12 pp.

Sims, P.K., Day, W.C., 1999. In: Klein, T. (Ed.), Geologic map of Precambrian rocks of the Hartville Uplift, Southern Wyoming with a section on Mineral Deposits in the Hartville Uplift. US Geol. Surv. Misc. Invest. Ser. Map I-2661, pp. 1–28.

Sims, P.K., Day, W.C., Snyder, G.L., Wilson, A.B., 1997. In: Peterman, Z.E. (Ed.), Geologic Map of Precambrian Rocks along part of the Hartville Uplift, Guernsey and Casebier Hill Quadrangles, Platte and Goshen Countries, Wyoming with a section on Geochronology of Post-tectonic Intrusive Rocks. US Department of the Interior US Geol. Surv. Misc. Invest. Series Map I-2567.

Smith, M.D., Heaman, L.M., 1999. Constraints on the timing of felsic magmatism associated with the Matachewan igneous events: preliminary results for the Creighton granite, Ontario, Geol. Ass. Canada, Min. Ass. Can. Joint Ann. Meeting Abst. 24, 119.

Snyder, G.L., Siems, D.F., Grossman, J.N., Ludwig, K.R., Nealey, L.D., 1995. Geology, petrochemistry, and geochronology of the Precambrian rocks of the Fletcher Park-Johnson Mountain area, Albany and Platte counties. In: Chamberlain, K.R., Snyder, G.L (Eds.), Wyoming with a section on the Fletcher Park Shear Zone by Frost. US Geol. Surv. Misc. Inv. Ser. Map I-2233, scale 1:24,000, 3 sheets.

Sozinov, N.A., Kazantsev, V.A., 1978. Phosphorite content of Proterozoic deposits in the Kursk Magnetic Anomaly (KMA) region. Lithol. Mineral Resourc. 13, 125–128.

Sozinov, N.A., Chistyakova, N.N., Kazantsev, V.A., 1988. Metallogenic Black Shales of the Kursk Magnetic Anomaly. Nauka, Moscow, p. 149.

Sreenivas, B., Das Sharma, S., Kumar, B., Patil, D.J., Roy, A.B., Srinivasan, R., 2001. Positive $\delta^{13}C$ excursion in carbonate and organic fractions from the Paleoproterozoic Aravalli Supergroup, northwestern India. Precambrian Res. 106, 277–290.

Stiller, M., Rounick, J.S., Shasha, S., 1985. Extreme carbon-isotope enrichments in evaporating brines. Nature 316, 434–435.

Swart, Q.D., 1999. Carbonate rocks of the Paleoproterozoic Pretoria and Postmasburg Groups, Transvaal Supergroup. M.S. Thesis. Rand Africans University, Johannesburg, South Africa, 126 pp.

Talbot, M.R., Kelts, K., 1986. Primary and diagenetic carbonates in the anoxic sediments of Lake Bosumtwi, Ghana. Geology 14, 912–916.

Valley, J.W., O'Neil, J.R., 1984. Fluid heterogeneity during granulite facies metamorphism in the Adirondacks: stable isotope evidence. Contr. Mineral. Petrol. 85, 158–173.

Van Cappellen, P., Ingall, E.D., 1994. Benthic phosphorus regeneration, net primary production, and ocean anoxia: a model of the coupled marine biogeochemical cycles of carbon and phosphorus. Paleoceanography 9 (5), 677–692.

Varentsov, I.M., Rakhmanov, V.P., 1980. Manganese deposits of the USSR: a review. In: Varentsov, I.M., Grasselly, G. (Eds.), Geology and Geochemistry of Manganese, E. Schweizerbart'sche Verlagsbuchhandlung (Nagele U. Obermiller), Stuttgart, pp. 319–391.

Veizer, J., Clayton, R.N., Hinton, R.W., 1992a. Geochemistry of Precambrian carbonates. IV. Early Paleoproterozoic (2.25 ± 0.25 Ga) seawater. Geochim. Cosmochim. Acta 56, 875–885.

Veizer, J., Plumb, K.A., Clayton, R.N., Hinton, R.W., Grotzinger, J.P., 1992b. Geochemistry of Precambrian carbonates. V. Late Paleoproterozoic seawater. Geochim. Cosmochim. Acta 56, 2487–2501.

Walraven, F., 1997. Geochronology of the Rooiberg Group, Transvaal Supergroup, South Africa. Econ. Geol. Res. Unit, University of the Witwatersrand, Inf. Circ. 316, Johannesburg, South Africa, 21 pp.

Weber, F., 1972. The Origin and Post-sedimentary Evolution of Precambrian Manganese Deposits of Moanda in the Republic of Gabon, Geology and Genesis of Precambrian Iron and Manganese Formations of the World. Naukova Dumka, Kiev, pp. 320–332.

Weber, F., 1997. Evolution of lateritic manganese deposits. In: Paquet, H., Clauer, N. (Eds.), Soils and Sediments, Mineralogy and Geochemistry. Springer, New York, pp. 97–124.

Weber, F., Schidlowski, M., Arneth, J.D., Gauthier-Lafaye, F., 1983. Carbon isotope geochemistry of the lower Proterozoic Francevillian series of Gabon (Africa). Terra. Cognita 3, 220 (Abstract).

Woodhead, J.D., Hergt, J.M., 1997. Application of the 'double spike' technique to Pb-isotope geochronology. Chem. Geol. 138, 311–321.

Yatsenko, G.M., Lavrenko, E.I., Mamchur, G.P., Rosikhina, A.I., 1986. Genesis of graphite in Precambrian formations of Inguletzk region and Krivoi Rog. Mineralogicheskii Sbornik 40 (1), 80–85.

Young, G.M., 1973. Tillites and aluminous quartzites as possible time markers for middle Precambrian (Aphebian) rocks of North America. In: Young, G.M. (Ed.), Huronian Stratigraphy and Sedimentation. Geol. Assn. Can. Spec. Pap.12, pp. 97–127.

Young, G.M., 1983. Tectono-sedimentary history of early Proterozoic rocks of the northern Great Lakes region. In: Medaris Jr., L.G. (Ed.), Early Proterozoic Geology of the Great Lake Region. Geol. Soc. Am. Mem. 160, 1983, pp. 15–32.

Young, G.M., 1991. The geologic record of glaciation: relevance to the climatic history of Earth. Geosci. Can. 18 (3), 100–108.

Yudin, N.I., Arsenev, A.A., 1970. Phosphate Content in Old Units in the Southern Part of Eastern Siberia. Nauka, Moscow, p. 123.

Yudovich, Y.Y., Makarikhin, V.V., Medvedev, P.V., Sukhanov, N.V., 1990. Carbon isotopic anomalies in carbonates of Karelian Series. Geochemistry (7), 972–978.

Yur'ev, L.D., 1968. Phosphate perspectives of old deposits of the Ukrainian Shield. Razvedka i Okhrana Nedr 11, 7–9.

Zagnitko, V.N., Lugovaya, I.P., 1985. Application of oxygen and carbon isotopes to some geologic problems in the Precambrian of the Ukranian Shield. Geochem. Ore Formation 13, 45–52.

Zagnitko, V.N., Lugovaya, I.P., 1986. Isotopic composition of graphite in rocks of the Ukrainian Shield. Minerol. J. 8 (1), 44–56.

Zagnitko, V.N., Lugovaya, I.P., 1989. Isotope Geochemistry of Carbonate and Banded Iron Formation Rocks from Ukraine Shield. Nauka Dumka, Kiev, p. 316.

Zhmur, S.I., Stepanova, N.A., 1987. Conditions of carbonaceous rock accumulation in the Oskol'sk Series of the Lower Proterozoic in the Kursk Magnetic Anomaly (KMA) and their analogues in the Phanerozoic. Lithol. Mineral. Resourc. 22 (6), 606–615.